Geoderma 450 (2024) 117045

Contents lists available at ScienceDirect

Geoderma

journal homepage: www.elsevier.com/locate/geoderma

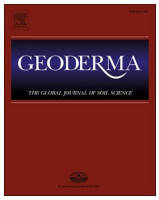

Forest catchment structure mediates shallow subsurface flow and soil base cation fluxes

Amanda Pennino [a,b,*], Brian D. Strahm [b], Kevin J. McGuire [b,c], Jennifer A. Bower [d], Scott W. Bailey [b], Madeline E. Schreiber [e], Donald S. Ross [f], Stephanie A. Duston [b], Joshua R. Benton [b,g]

[a] UDSA-NRCS, National Soil Survey Center, 100 Centennial Mall North, Lincoln, NE 68508, USA
[b] Virginia Tech, Dept. of Forest Resources and Environmental Conservation, Cheatham Hall, Blacksburg, VA 24061, USA
[c] Virginia Water Resources Research Center, 210 Cheatham Hall, Blacksburg, VA 24061, USA
[d] Soil Health Institute, 2803 Slater Rd Suite 115, Morrisville, NC 27560, USA
[e] Virginia Tech, Dept. of Geosciences, Derring Hall, Blacksburg, VA, USA
[f] University of Vermont, Department of Plant and Soil Science, 260 Jeffords Hall, Burlington, VT 05405, USA
[g] United States Geological Survey, Reston, VA, USA

ARTICLE INFO

Keywords:
Forest soils
Nutrients
Mineral weathering
Groundwater
Hubbard Brook
Critical Zone Science

ABSTRACT

Hydrologic behavior and soil properties across forested landscapes with complex topography exhibit high variability. The interaction of groundwater with spatially distinct soils produces and transports solutes across catchments, however, the spatiotemporal relationships between groundwater dynamics and soil solute fluxes are difficult to directly evaluate. While whole-catchment export of solutes by shallow subsurface flow represents an integration of soil environments and conditions but many studies compartmentalize soil solute fluxes as hillslope vs. riparian, deep vs. shallow, or as individual soil horizon contributions. This potentially obscures and underestimates the hillslope variation and magnitude of solute fluxes and soil development across the landscape. This study determined the spatial variation and of shallow soil base cation fluxes associated with weathering reactions (Ca, Mg, and Na), soil elemental depletion, and soil saturation dynamics in upland soils within a small, forested watershed at the Hubbard Brook Experimental Forest, NH. Base cation fluxes were calculated using a combination of ion-exchange resins placed in shallow groundwater wells (0.3 – 1 m depth) located across hillslope transects (ridges to lower backslopes) and measurements of groundwater levels. Groundwater levels were also used to create metrics of annual soil saturation. Base cation fluxes were positively correlated with soil saturation frequency and were greatest in soil profiles where primary minerals were most depleted of base cations (i.e., highly weathered). Spatial differences in soil saturation across the catchment were strongly related to topographic properties of the upslope drainage area and are interpreted to result from spatial variations in transient groundwater dynamics. Results from this work suggest that the structure of a catchment defines the spatial architecture of base cation fluxes, likely reflecting the mediation of subsurface stormflow dynamics on soil development. Furthermore, this work highlights the importance of further compartmentalizing solute fluxes along hillslopes, where certain areas may disproportionately contribute solutes to the whole catchment. Refining catchment controls on base cation generation and transport could be an important tool for opening the black box of catchment elemental cycling.

1. Introduction

Base cations (i.e., Ca, Mg, Na, and K) are of interest to pedologists, biogeochemists, ecologists, and hydrologists alike for their important role in soil development and nutrient status and buffering capacity to neutralize acidity. Quantifying pools and fluxes of base cations is particularly important for eastern North American and European forests that experienced decades of acid rain, resulting in a depletion of soil base cation pools due to leaching to streams (Likens et al., 1996; Lawrence et al., 2016; Watmough et al., 2005). This subsequently altered

* Corresponding author at: UDSA-NRCS, National Soil Survey Center, 100 Centennial Mall North, Lincoln, NE 68508, USA.
E-mail address: amanda.pennino@usda.gov (A. Pennino).

https://doi.org/10.1016/j.geoderma.2024.117045
Received 8 March 2024; Received in revised form 28 August 2024; Accepted 19 September 2024
Available online 25 September 2024

forest composition and surface water quality. Soil base cation fluxes are reflective of many dynamic ecosystem processes (e.g., atmospheric deposition, mineral dissolution, biotic uptake, soil exchange and leaching) that impact the trajectory of soil development and function. Soil forming processes critically depend on soil water to transport, translocate, and transform solid and dissolved material (Simonson, 1959; Lin, 2010). As such, rates of pedogenesis have often been, directly or indirectly, related to hydrologic fluxes (e.g., Dixon et al., 2016; Maher, 2010; White and Blum, 1995). While catchment characteristics (e.g., topography, soil properties) and the soil hydroclimate are known to co-vary (Bailey et al., 2014; Bower et al., 2023a; Lin et al., 2006), there is currently a lack in the understanding of how these together influence spatial patterns of soil base cation fluxes. Quantifying these relationships is important for constraining rates of soil development, watershed geochemical fluxes, and resilience to ecosystem disturbances.

It is well established that hillslope topography (e.g., surface and subsurface form, slope, and structure) and soil properties (e.g., permeability, thickness) are important controls on the spatiotemporal organization of soil–water interactions because they affect water flow paths (Beven and Germann, 1982; Jencso et al., 2009; Welsch et al., 2001; Weiler et al., 2006; Western et al., 1999) and by extension, water residence and travel times (Maher, 2011; McGuire et al., 2005; Tetzlaff et al., 2009; Xiao et al., 2021). In mountainous forested landscapes, steep hillslopes are often dominated by permeable shallow soils, which can promote the formation of shallow water tables and lateral subsurface flow paths during storm events and snowmelt (Freer et al., 2002; Jackson, 1992; Whipkey, 1965). Analogous to the horizontal formation of soil horizons within soil pedons, water fluxes in the lateral direction leads to the mobilization, translocation, and accumulation of solutes downslope from their point of origin (generation), such as described by lateral podzolization (Bailey et al., 2014; Jankowski, 2014; Park and Burt; 2002; Sommer et al., 2000; 2001). Shallow subsurface flow (also known as lateral flow, interflow, throughflow, subsurface runoff, etc.), a mixture of soil pore water and transient groundwater, is considered a significant runoff generation mechanism in forested headwater catchments (Anderson and Burt 1978; Chifflard et al. 2019; Hewlett and Hibbert, 1967; Pearce et al., 1986; Weiler et al. 2006) and results in hydrologic connectivity between upper and lower areas of the catchment and the rapid transport of solutes to adjacent streams (Bracken and Croke, 2007; Jencso et al., 2009; Klaus and Jackson, 2018; McGlynn and McDonnell, 2003).

While shallow subsurface flow is a recognized mechanism by which soil water reaches streams, direct quantification of lateral base cation fluxes from hillslope soil source waters and their relative contribution to whole-catchment export is currently lacking (Johnson et al., 2000; Tokunaga et al., 2022). When catchments wet up, the composition of the percolating water continually transforms as flow paths and contributing areas shift and groundwater interacts with different soil components with varying chemistries. For this reason, solute fluxes vary across catchments and within soils themselves.

Variations in stream solute export as a function of discharge (e.g., concentration discharge (C-Q) relationships) justify the notion that soil–water contact time and solute sources shift across flow conditions (Knapp et al., 2020; Godsey et al., 2009), inferring that catchment export is reliant on both reaction rates and the heterogeneity of the catchment itself (Musolff et al., 2021). To identify geographic source areas of soil water to receiving steams, studies have applied hydrograph separation techniques and end-member mixing models using chemical or isotopic tracers to solve a mass balance for a predetermined set of flow components (Buttle, 1994; Christophersen and Hooper, 1992; Klaus and McDonnell, 2013; Pinder and Jones, 1969). Often, end members are simplified into either two distinct time components: event and pre-event water; or two depth components: deep or shallow groundwater (e.g., soil water) (Bazemore et al., 1994; Hooper et al., 1990; Stewart et al., 2022). Rarely is the shallow flow component separated into multiple subcomponents beyond upland versus riparian areas (Burns et al., 2001; Garrett et al., 2012; Inamdar and Mitchell, 2006; 2007). What is missing from many modelling approaches are spatiotemporally distributed hillslope measurements of shallow water table dynamics and groundwater chemistry (Kim et al., 2017; Li et al., 2017), which can be extremely variable across forested catchments (Bailey et al., 2019; Benton et al., 2022; Kiewiet et al., 2019; Gannon et al., 2014).

In this study we aim to characterize the spatial patterns of annual base cation fluxes through variably saturated shallow soil (<1 m deep) in upland areas of a forested catchment. We hypothesize that spatial variations in shallow subsurface flow dynamics, which can regulate solute generation and transport, will result in a predictable configuration of base cation fluxes along hillslopes. To test this hypothesis, we evaluate the explanatory power of metrics that describe shallow groundwater dynamics on base cation fluxes associated with mineral weathering reactions. Additionally, we investigate linkages between catchment properties that predict groundwater behavior and observed differences in elemental depletion. We use these data as evidence that base cation fluxes and soil developmental processes in the shallow soil zone are neither uniform nor random, but rather exist in a systematic spatial arrangement determined by the structure of a catchment's topography and hydrology.

2. Materials and methods

2.1. Site description and experimental design

This study took place at the Hubbard Brook Experimental Forest (HBEF), in Watershed 3, a hydrologic reference catchment (e.g, no experimental manipulations) (Fig. 1). The HBEF, located in the White Mountains of New Hampshire, has a cool temperate, humid-continental climate with an average of 1,400 mm of precipitation annually (Bailey, 2003). The catchment at lower elevations is dominated by northern hardwoods, including sugar maple (*Acer saccharum*), yellow birch (*Betula alleghaniensis*), American beech (*Fagus grandifolia*), which transitions to red spruce (*Picea rubens*), balsam fir (*Abies balsamea*), and mountain paper birch (*Betula cordifolia*) at higher elevations.

The bedrock geology of Watershed 3 is dominated by schists of the Rangeley Formation, overlain by glacial till of variable depths that is composed primarily of Kinsman granodiorite. At HBEF, soils are predominantly classified as Spodosols (typic Haplorthods) with sandy loam textures and thick O/A horizons, and local areas of Inceptisols and Histosols (Bailey, 2003). Ridges and spurs within the catchment are dominated by bedrock outcrops and shallow-to-bedrock organic soils (Fraser et al., 2020). Intensive soil characterization in the region has produced soil maps comprised of distinct podzol types (i.e., hydropedological units) based on variations in spodic expression that generally occur in a downslope gradient from ridges to lower riparian areas (Gillin et al., 2015; Fraser et al., 2024; Fig. S1). Characteristic shallow groundwater saturation regimes (water table occurrence, persistence, and depth) associated with each soil map unit demonstrate that hydrologic behavior is an important soil-forming factor in upland positions at HBEF (Bailey et al., 2014; Gannon et al., 2017).

Three areas within the catchment were chosen as investigative transect sites for this study (Fig. 1). At each of the three transects, wells were installed at three different locations along the hillslope, targeting a range of upland soil map units (9 water level logging wells; Fig. S1). Wells were constructed using 51 mm (2 in.) diameter PVC with 51 mm (2 in.) of PVC screen (slot size 0.25 mm). Wells were placed within a small borehole and back filled with a small layer of local sand around the screen to reduce the effects preferential flow around the installed well. Wells were installed to the top of the C horizon, or if none existed, at the bedrock surface. For more information on well installation, refer to Benton et al. (2022). Previous work at this site suggests that the water table can perennially exist deeper in the C horizon (Detty and McGuire, 2010). The formation of the transient water table will frequently reach above the C horizon during conditions of high streamflow (e.g.,

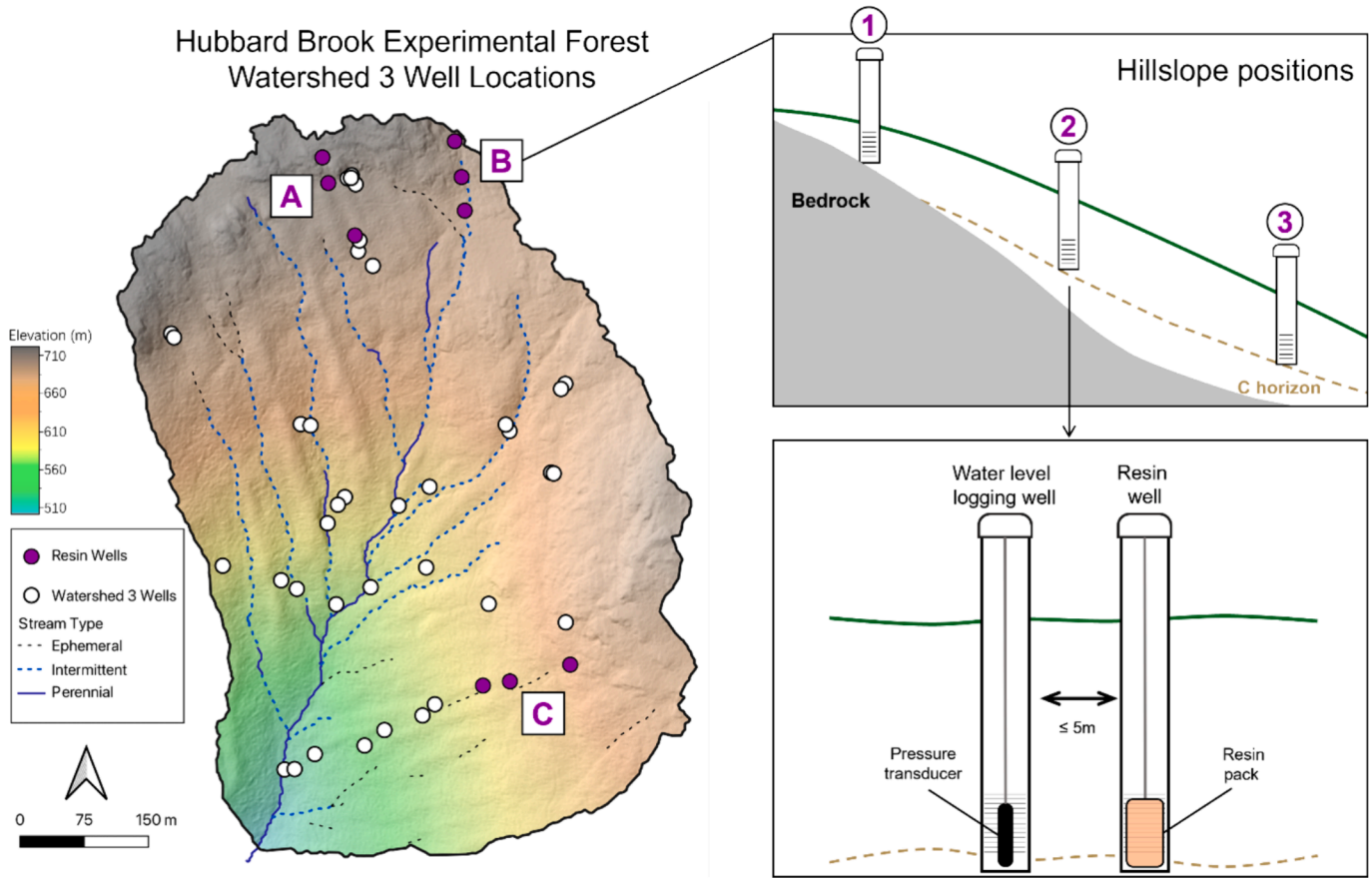

Fig. 1. Left: Digital elevation model (DEM) and hillshade of Watershed 3 at Hubbard Brook Experimental Forest, in New Hampshire (USA). Purple circles indicate the locations of the wells at three study transects (A-C) and white circles indicate wells that were installed prior to this study (data from 2010 to 2014). Top right: hillslope cross-section: Along each of the three transects, wells were installed in 2019 at three different hillslope locations (1–3) to the depth of the bedrock or C horizon interface. Bottom right: Each location had a well equipped with a pressure transducer to record water levels, and within five meters, another well where ion exchange resins were placed for the duration of this study.

precipitation and snowmelt events). A lower saturated hydraulic conductivity in the C horizon (10^{-8} to 10^{-6} m/s) compared to the solum above (10^{-6} to 10^{-4} m/s) suggests that water fluxes are likely greater in the shallow soil zone (Benton et al., 2022) and are of unique interest to separate from fluxes in the C horizon or deeper. Therefore, groundwater level measurements were collected in the shallow soil zone (i.e., above the C horizon). Groundwater levels were measured using pressure transducers (HOBO Onset U20 & U20L) at 10-minute intervals over the course of the study period (1 year). Raw pressure data were corrected for atmospheric pressure by using barometric pressure data from a pressure transducer suspended in a dry well (within Transect C, Fig. 1). Water level data for this site can be found in Bailey et al., (2024).

Within 5 m of each of the water level logging wells, narrow pits were carefully excavated to the same depth. After soil profile characterization and horizon sampling (described in Section 2.2), an additional well was installed within the pit to house ion-exchange resins for elemental mass flux measurements (Fig. 1).

2.2. Soil characterization and analysis

Soil profiles at all resin-well locations were morphologically characterized and sampled by genetic horizon using the criteria of Schoeneberger et al. (2012). Samples of each mineral horizon within the soil profile (n = 28 samples) were air-dried and then sieved to <2 mm. For all samples, 20 g of each sample were sent to Activation Laboratories (Ancaster, Canada) to be analyzed for elemental concentrations of Ca, Na, Mg, and Al. Samples were fluxed with lithium metaborate/tetraborate, diluted in a nitric acid solution and then analyzed by inductively coupled plasma optical emission spectroscopy (ICP-OES) (Kowalenko & Babuin, 2014).

Elemental data for fourteen C horizon samples from 1 to 6 m in depth within Watershed 3 were also analyzed and average concentrations were used as a proxy for unweathered parent material (Bower et al., 2023a; Bower et al., 2023b). Elemental enrichment or depletion factors were determined by calculating tau values (τ) for each *i*th element (τ_i) (Brimhall and Dietrich, 1987) using the following equation:

$$\tau_i = \frac{i_{w \times Ti_w}}{i_p \times Ti_p} - 1 \quad (1)$$

Values where $\tau > 0$ indicate elemental mass gain (enrichment) and $\tau < 0$ indicate mass loss (depletion) of weathered material (subscript *w*) in mobile element, *i*, in relation to unweathered reference parent material (subscript *p*). Mobile elemental concentrations were indexed to titanium (Ti), which is found in higher abundance, minimally biogeochemically cycled, and resistant to dissolution compared to Zr, Y, and Rb in these soils (see: Bower et al., 2023b).

In addition to the nine excavated soil pits (locations of resin wells), a campaign aimed at describing shallow soil horizon distribution (above the C horizon) took place during 2018 and 2019. Auger investigations surrounding the three study transect locations occurred at a fine-scale gridded resolution (~5–10 m) were used to describe soil horizon presence/absence, color, and thickness. The purpose of this auger investigation was to create average soil volume estimations for each horizon by multiplying the mean horizon thickness (m) with the total area (ha) for

the upslope drainage area above the resin well locations. A total of 408 auger holes were dug (Fig. S2) and upslope areas were determined using "watershedding" methods described in Section 2.5.

2.3. Ion-exchange resins and base cation flux estimations

Characterization of shallow groundwater chemistry is difficult when the transient water table may only exist for a few hours or less during a storm event. Additionally, chemistry at a single location can vary both seasonally and with storm event magnitude. Therefore, we deployed ion-exchange resins within wells to measure time-integrated groundwater chemistry. As water passes through the well, solutes of interest are adsorbed onto resin beads and a tracer compound is released. In theory, intersecting water flows freely into and out of the resin pack, which has a hydraulic conductivity that is at least as high as the surrounding, native soil, although this work did not measure any potential interference from flow convergence/divergence around the well in the field or as a laboratory experiment. However, the application of resins within screened PVC wells to measure solute mass fluxes in groundwater is based on the passive flux meter, which has been extensively described and laboratory evaluated (Annable et al., 2005; Campbell et al., 2006; Hatfield et al., 2004; de Jonge & Rothenberg, 2005). Additionally, the use of ion exchange resins to measure nutrient load in terrestrial ecosystems and variably saturated soil has been applied widely across soil science to measure nutrient availability (e.g., Johnson et al., 2005; Kjønaas, 1999; Lehmann et al., 2001; Willich and Buerkert, 2016).

We used Amberlite IR-120H+form resins (strongly acidic), that were pretreated with 2 *M* KCl by combing the salt solution and resin at a 3:1 solution-to-resin weight ratio and shaken on a fixed-speed reciprocal shaker (Eberback Model E6010) at 180 oscillations min^{-1} (low speed) for two hours. After allowing the resin to settle, the supernatant was decanted, and resins were rinsed with DI water three times to remove excess salts. Approximately 90 g of resin (moist) was assembled into each resin pack, which was encased in permeable mesh nylon wrapped around two rubber washers (OD: 51 mm, ID: 16 mm), along a 13 mm (½ inch) CPVC pipe, then sealed with electrical tape and kept moist at 4 °C until deployment (Fig. 2). Approximately 400 g of pretreated resin was reserved and kept at 4 °C to use as blanks to test resins for any background element contributions from resin degradation over time.

Resin packs were attached to a nylon string and pushed down into the wells across all transects. The resin packs sat at the bottom of each well within the screened section of PVC pipe (Fig. 1, Fig. 2), which allowed for lateral water flow through the well and interception with the resin pack. Resin packs were exchanged four times, with deployment periods ranging from 2-4 months each, for a total of one year integration from August 2019–2020.

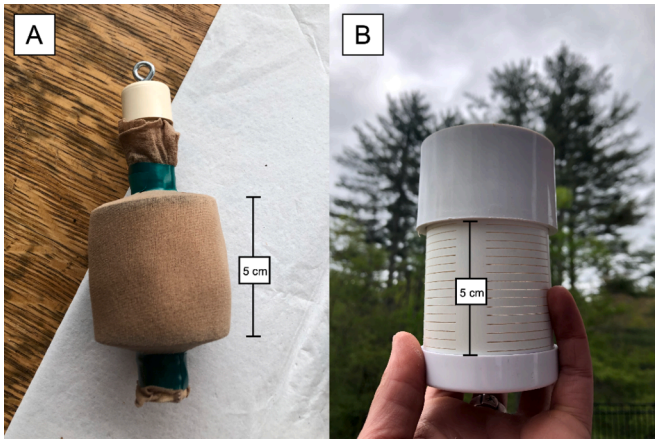

Fig. 2. Photographs of ion-exchange resin packs, which were encased within nylon attached to CPVC piping (A). Resin packs were pushed down into slotted screens attached at the bottom of each well (B) to allow the lateral flow of water through the resin pack.

Following each resin deployment, resins were brought back to the lab and each resin pack was opened, weighed for total moist mass and subsampled to 20 g (wet weight), with 3 replicates. Subsamples were extracted with 2 *M* KCl following similar protocols to pretreatment, using a 3:1 solution-to-resin ratio, and shaken for 2 h. Subsamples went through 2 subsequent extractions to ensure all sorbed solutes were retrieved from the resin beads. Extractant solutions were analyzed for Ca, Mg, and Na using an ICP-MS. These ions were chosen due to their abundance in minerals that are preferentially weathered in this region (e.g., plagioclase, biotite, and chlorite), and are the primary and largest weathering source of cations in the shallow soil zone. The use of KCl as the extractant limited our ability to measure sorbed K ions on the resins, although potassium (K) exists in less weatherable minerals in this region (such as microcline and muscovite). Any mass extracted from the resin blanks was subtracted from the extractant's value, which were all measured at <1 mg/L for all elements of interest. Calculations and total mass of each solute extracted from these resins for the total year can be found in Pennino et al. (2023). The mass of solute in solution from each resin subsample extractant was averaged to a single value, then scaled to represent the total weight of the resin in the resin pack. On a per-element basis, each deployment mass was then summed for all deployment periods (successive deployments for one year) for each resin location. Total elemental mass (scaled to kg) was divided by deployment time (one year) to calculate the annual mass solute flux (kg yr^{-1}) at each location where the resins were deployed.

Annual mass fluxes (kg yr^{-1}) were divided by the upslope drainage area (ha), with the assumption that all water within this area flows through a central point at the resin location. Area-normalized solute fluxes (kg ha^{-1} yr^{-1}) were then scaled to represent a 2-D plane of water moving through each resin pack. The height dimension of each plane was determined by scaling the height of resin intercepting water to the average height of a water table response. Mean annual water levels for each resin location were taken from the nearest water level logging well to the resin. The width dimension of the plane was determined by scaling the width of the resin to a 1-m wide contour on the landscape. For the terms used in these calculations, refer to Supplementary Materials Table S1. The largest source of uncertainty involved in calculating base cation fluxes comes from the estimation of average water table height in a location (See Section 2.3), which was used to scale mass fluxes to an entire water column within a soil profile. Due to the inherent variability of water table fluctuations (Table S1) this introduces approximately 30–80 % of uncertainty around the measurement of these fluxes.

2.4. Metrics of shallow groundwater behavior

To test the effects of hydrologic heterogeneity on the spatial variations in base cation fluxes, we measured shallow groundwater levels during the length of the study in the same nine locations where resins were located. We compared the calculated groundwater metrics to topographic information (e.g., slope, curvature) and other catchment properties that have been shown to be useful for predicting spatial patterns in soil development at Hubbard Brook (Gillin et al., 2015).

For this study we calculated hydrograph metrics that reflect the annual dynamic behavior of the transient groundwater table: saturation frequency, saturation duration, and mean response depth, for multiple depths in the soil profile. We define saturation frequency as the number of times the transient water table crossed a threshold depth beneath the surface per year (saturation cycles/yr), where one saturation cycle indicates the groundwater levels rose to and then receded past that depth in the soil profile once. Similarly, saturation duration was calculated as the proportion of time the water table existed at or above a depth during a logging period. Average water level response depth (from the soil surface) was calculated for when the water table was present within the

soil profile. Larger response depths indicate, on average, a deeper water table. Prior to any metric calculation, 10-min water levels were smoothed by aggregating them to two-hour mean values. To test the influence of depth, saturation characteristics were calculated at 5-cm intervals from the soil surface to the depth of the shallowest well (30 cm): at 5, 10, 15, 20, 25, 30 cm. If time gaps in the data logging existed, saturation metrics were scaled to a full year.

2.5. Calculation of catchment topographic and soil attributes

Topographic attributes for each resin location in Watershed 3 were calculated using R (RStudio Team, 2020), QGIS (QGIS Development team, 2021), and ArcGIS software and derived from a DEM. The full list of topographic metrics and value ranges for well networks can be found in Table 1 and additional maps of attributes can be found in the Supplementary Materials (Fig. S3). The 5-m DEM for Watershed 3 (Fraser et al., 2022) was prepared for hydrologic analyses by Fill Depressions (Wang and Liu, 2006) and Least Cost Depression Breaching (Lindsay, 2014) prior to performing the watershedding operation. Pour points were snapped to a flow accumulation grid created from a D8-derived flow direction raster to map areas that drain to each point. Sub-watershed borders (upslope drainage areas) were manually adjusted for known surface artifacts and onsite expert knowledge of the landscape to create upslope areas for each resin and groundwater level logging well locations.

Topographic properties included those calculated at well locations (local pixel value) and for the upslope drainage area (mean value across the area) (cf. Rinderer et al., 2014). The use of mean upslope area values, rather than local values, allowed us to examine topographic properties at a broader scale and to account for the effects of the form and length of upslope flow paths on downslope water level dynamics. Listed attributes with 'upslope mean' were calculated as the mean value for the spatial extent of the upslope drainage area. Upslope drainage area determined for each well location was derived using the watershed function in WhiteBoxTools in R (Lindsay, 2014). This tool performs a watershedding operation based on designated outlet pour points (resin locations).

For this study, topographic wetness index (TWI), which describes the spatial redistribution of water based on specific catchment area and slope, was calculated using the downslope gradient instead of local slope of the cell (i.e., the gradient was based on the horizontal distance to a downslope cell with an elevation 5 m below the elevation of the starting cell) to reduce the potential influence of microtopography (Hjerdt et al., 2004; Seibert et al., 2007; Gillin et al., 2015).

Upslope accumulated area (UAA) was calculated as the number of cells contributing to a single point based on the multiple flow direction method (Seibert and McGlynn, 2007). A weighted UAA (UAAw) was created by assigning an arbitrarily large weighting value (10^5) for cells that were bedrock outcrops and zero for non-bedrock outcrops. Weights were used as a multiplier for the accumulated area calculation in the weighting function of the SAGA recursive catchment area tool. If weights were less than 1, then flow accumulation would be reduced in the downslope direction. However, making the weighting value large increases the effect as the area accumulates. A normalized ratio between the weighted UAA (UAAw) and unweighted UAA (i.e., all weights set to 1) was used to calculate bedrock-weighted UAA (UAAb) (Gillin et al., 2015; Fraser et al., 2020). The UAAb metric varies between 0–1, where a value of 1 indicates an entire upslope area is comprised of bedrock outcrops and associated shallow, organic soils. This metric was shown to be useful for identifying soils that may have been formed through lateral podzolization processes (Gillin et al., 2015).

For each resin well location, depth-weighted means of profile elemental depletion (tau; τ) were calculated for all mineral horizons above the C horizon. Using horizon depth data collected from the extensive auger investigations (Section 2.2 and Fig. S2), the proportion of upslope soil horizon volume for E and B horizons was calculated. To do this, total upslope soil volume was determined by finding an average depth to the C horizon, or bedrock if there was none, for each upslope drainage area from the resin location. The average thickness of the B and E horizon within each area was used to determine proportions of each soil horizon out of the total solum volume.

To test if relationships between groundwater metrics and catchment attributes at the resin wells (n = 9 locations) were similar to metrics/attributes at well locations across the catchment, we analyzed water level data from an additional 43 wells installed throughout the catchment by Detty and McGuire (2010), Gannon et al. (2014), and Benton et al. (2022) between 2008–2019. Chosen wells for this study met the following two qualifications: at least one or more years of consecutive water level data and installed into similar shallow soil depths (at or above the C horizon).

2.6. Statistical analyses

The differences between base cation fluxes for each hillslope position and between transects were tested for significance using a one-way analysis of variance test (ANOVA) at a significance level of $p < 0.05$. As an exploratory analysis, simple linear regression models were used to fit relationships between total base cation fluxes (log transformed) and hydrodynamic variables (n = 9) using the R software 'stats' package (R Core Team, 2021). The best fit models for saturation frequency and duration were selected based on the highest r^2 value. The top models chosen for saturation frequency and duration at resin locations were

Table 1
Ranges in locally derived and upslope drainage area mean values of topographic attributes. Transect wells are located near deployed resins (Fig. 1) and are included in the range of values for all Watershed 3 wells.

Variable	Metric	Topographic characteristic	Reference	Value range (Resin wells) n = 9	Value range (All Watershed 3 wells) n = 43
DISTOUT	Linear distance to catchment outlet (m)	Local	QGIS	7–172	7–267
ELEV	Elevation (m)	Local	Fraser et al. (2022)	602–710	529–708
TPI	Topographic position index, 100 m window	Upslope mean	Guisan et al. (1999)	1.5–5.8	−1.3–8.4
UAA	Multiple direction- upslope flow accumulation	Upslope mean	SAGA; Seibert and McGlynn (2007)	57–420	57–2231
UAAb	UAA, weighted by areas of bedrock and shallow soils (unitless)	Local	Gillin et al. (2015)	0.2–0.6	0–0.6
SLOPE	Downslope gradient (degrees)	Upslope mean	Hjerdt et al. (2004)	0.17–0.36	0.12–0.42
PROF	Profile curvature	Upslope mean	QGIS	$-1.7{\cdot}10^{-3}$–$7.1{\cdot}10^{-3}$	$-1.3{\cdot}10^{3}$–$8.1{\cdot}10^{-3}$
PLAN	Planar curvature	Upslope mean	QGIS	$-2.0{\cdot}10^{-3}$–$4.3{\cdot}10^{-2}$	$-2.0{\cdot}10^{-3}$–$6.6{\cdot}10^{-2}$
CONVERGE	Convergence index	Upslope mean	SAGA	−0.4–4.3	−0.3–4.3
TWI	Topographic Wetness Index, using 5 m downslope gradient for slope (ln(m^2))	Upslope mean	SAGA; Hjerdt et al., (2004)	5.9–6.9	5.8–7.4

used in a Spearman rank correlation analysis (Spearman, 1904) with local and upslope drainage area properties calculated for the resin well locations, using the 'Hmisc' package in R software Version 4.2.2 (R Core Team, 2021). To investigate the strength of correlates beyond the limited number in wells associated with resin locations (n = 9; Fig. 1 in purple), we ran a second Spearman correlation analysis using topographic attributes and hydrodynamic properties for the extended well network of Watershed 3 (n = 43; Fig. 1 in white and purple). Significance between Spearman correlates denoted by $p < 0.05$ signifies p-values between 0.01–0.05 and $p < 0.01$ signifies p-values between 0.001–0.01.

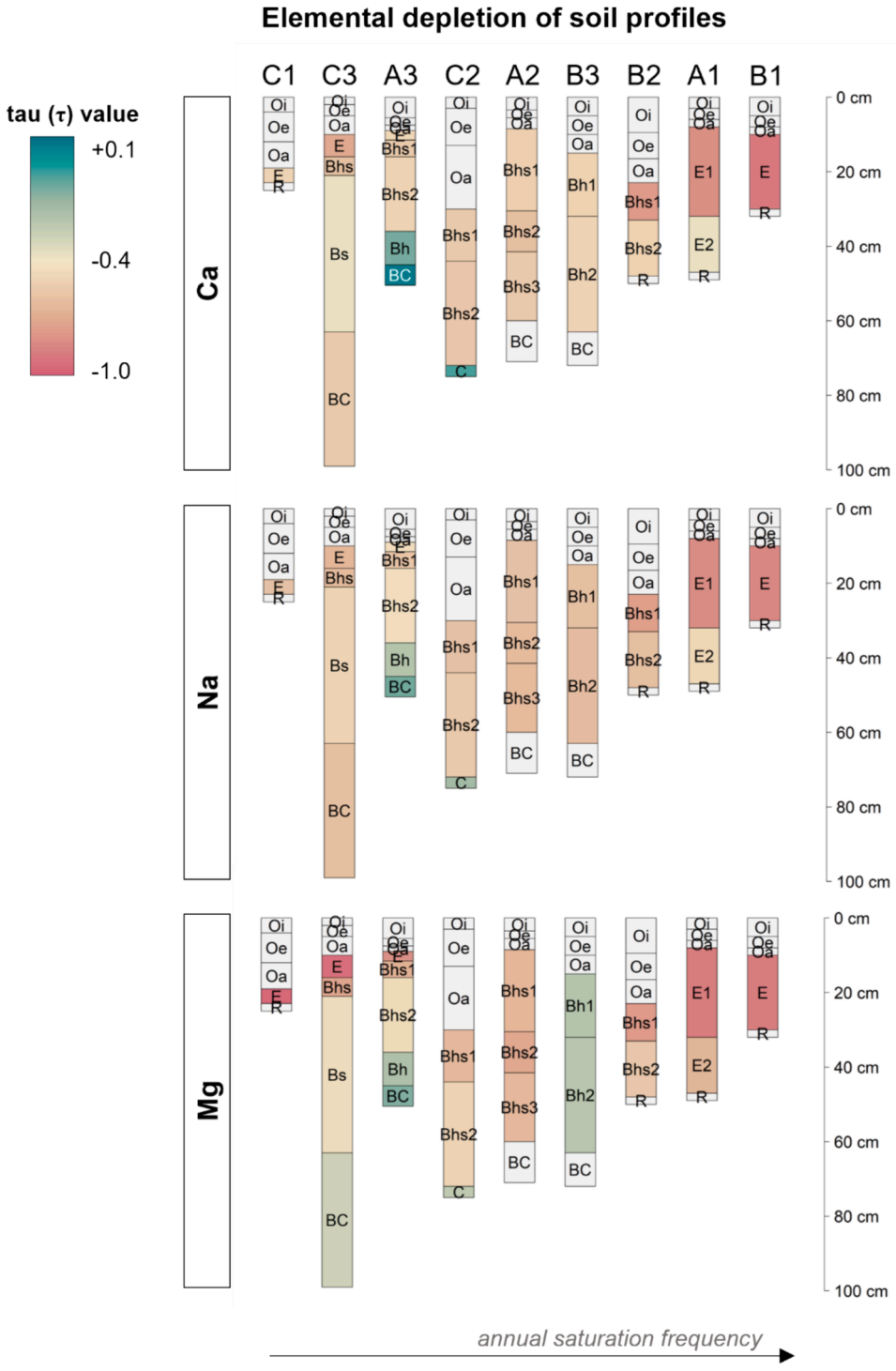

Fig. 3. Horizons described in soil profiles within transects A-C along hillslope positions 1–3 color coded by soil elemental depletion (tau values (τ)). Soil profiles are arranged by the annual saturation frequency of each soil profile from left (low saturation frequency) to right (high). Tau values that are increasingly negative are more depleted in that element and indicate a weathering loss. Gray boxes indicate tau values were not calculated due to insufficient mineral content, or where there was missing data. Tau values for aluminum can be found in the *Supplementary Materials* (Fig. S4).

3. Results

3.1. Soil morphology and weathering extent

The three hillslope positions (1–3) where base cations were measured comprised of an elevational gradient from higher catchment ridges (1) to mid and lower backslope positions (2 and 3). Soils located in hillslope position 1 were shallowest in depth to bedrock (23–47 cm) and exhibited an O-E horizon profile sequence directly on top of bedrock. Soils in hillslope positions 2 and 3 were generally thicker and reached down to a BC or C horizon (45–62 cm). All soil profiles in hillslope position 2 had thick and dominant Bhs horizons. Two out of the three soil profiles in hillslope position 3 exhibited a typical spodosol horizon sequence, including eluvial and illuvial spodic horizons (e.g., O-E-Bhs-Bs). Described soil profiles would classify as Humods, Orthods, or Folists (Soil Survey Staff, 2022). Full morphological descriptions of each soil profile can be found in Bower et al. (2023c) and the designation of how each soil profile was classified by the local hydropedological unit classification is shown in Figure S1.

Depth-weighted profile averages of elemental depletion (tau; τ) ranged from τ-Ca = −0.81 to −0.35, τ-Na = −0.77 to −0.38; τ-Mg = −0.87 to −0.25, and τ-Al = −0.60 to −0.25. The more negative tau values indicate greater elemental depletion (weathering loss). For all elements except for Mg, the B1 soil profile was most weathered and A3 was the least weathered (Fig. 3, Fig. S4). The C1 profile had the greatest loss of Mg, although, the proportion of mineral horizon thickness to organic horizons was extremely small. The B3 soil profile was least weathered of Mg. If present in the soil profile, the E horizon was the most elementally depleted horizon for all elements analyzed.

3.2. Annual soil base cation fluxes

The measured base cation fluxes varied greatly across the catchment. However, there were no statistical difference in base cation fluxes was found between hillslope positions (1–3) or transects (A-C). The largest flux estimates for total base cations occurred in hillslope position 1 for transects A and B, at 5.8 and 3.9 kg ha^{-1} yr^{-1}, respectively, and generally decreased downslope (Fig. 4). Conversely, total base cation fluxes for transect C were greatest in hillslope position (3) and decreased with increasing elevation, ranging only from 0.5 to 0.2 kg ha^{-1}yr^{-1}. Out of all the locations, position C1 had the lowest base cation flux. On average, Ca contributed 49 %, Na contributed 43 %, and Mg contributed only 8 %, towards the summed base cation flux.

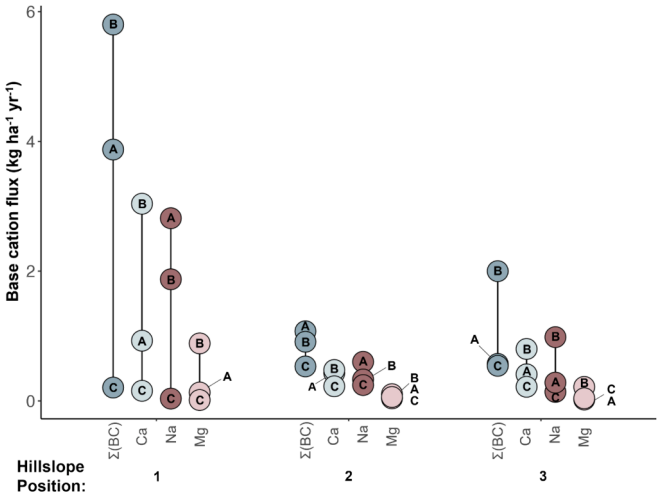

Fig. 4. Area-normalized annual solute fluxes (kg ha^{-1} yr^{-1}) for Ca, Na, Mg, and sum of base (∑(BC)) cations measured at three transect locations (A, B, C) at three different hillslope positions (1, 2, 3). The estimated uncertainty is approximately 30–80 %. See Fig. 1 for locations of transects and hillslope positions within the catchment.

3.3. Shallow groundwater metrics as predictors of base cation fluxes

Water table depth, persistence, and recession characteristics varied with hillslope position. Water levels in wells in the uppermost hillslope position (1) often exhibited "flashy" behavior, with rapid responses during high flow conditions (Fig. 5). On average, water levels in hillslope position 1 rose high into and receded completely from the soil profiles 36 times/yr (range of 29–61 saturation cycles/yr). While saturation occurred at a relatively high frequency, the duration of saturation throughout any part of the monitored soil profile was lower at position 1 (saturated 11–68 % of the year depending on depth; average 38 %). When groundwater was present in the shallow soil profile, the mean water table depth was 29 cm from the soil surface but ranged from 37 cm in depth to 0 cm (i.e., saturated to the surface).

At hillslope positions 2 and 3, the depth to the transient water table was often deeper and/or had slower a recession. For example, for locations B2 and B3, the water table was present in the soil profile for a longer duration of the year (83 % and 95 %, respectively; Fig. S5). The average response depth to the water table for positions 2 and 3 for all transects was 37 cm and 53 cm, respectively. In stark contrast to higher positions on the hillslope, the number of saturation cycles within soil profiles in the two lower positions for all transects was low, with a mean saturation frequency of 16 cycles/yr for position 2 (range of 5–32 cycles), and 9 cycles/yr for position 3 (range of 5–16 cycles).

Overall, saturation duration was a poor predictor of total base cation fluxes for all investigated depths ($r^2 \leq 0.22$; $p = 0.11$–0.55) compared to saturation frequency (Fig. S7). Generally, total base cation and individual cation fluxes increased exponentially with an increased frequency in saturation (Fig. 6). The number of saturation cycles at or below 15 cm from the surface were strong predictors ($r^2 \geq 0.54$; $p < 0.05$) whereas shallower depths were not ($r^2 \leq 0.20$; $p = 0.12$–0.70). The predictive power of saturation frequency on log transformed total base cation fluxes was greatest for the water table rise threshold of 20 cm from the surface ($r^2 = 0.86$; $p < 0.001$; Fig. S7).

3.4. Correlations between fluxes, groundwater metrics, and topography

Total base cation fluxes and saturation frequency were correlated to similar catchment properties. Base cation fluxes were strongly and significantly correlated to the distance from the catchment outlet (DISTOUT; $r_s = 0.89$, $p < 0.01$) and saturation frequency ($r_s = 0.89$, $p < 0.01$; Fig. 7). In general, the three sites farthest from the catchment outlet (i.e., higher elevation portions of the catchment) were most periodically saturated to shallow depths (>25 cycles/yr) and had total base cation fluxes > 1 kg ha^{-1} yr^{-1}. Soils draining to these sites typically had a greater upslope volume of E-horizon, as a fraction of the total solum, and the highest proportion of upslope accumulated area weighted by bedrock and shallow-to-bedrock regions (UAAb > 57 %).

There were significant and negative correlations between the number of soil saturation cycles and the mean upslope topographic wetness index (TWI; $r_s = -0.74$, $p < 0.05$) and flow accumulation (UAA; $r_s = -0.64$, $p < 0.05$), which are topographic-derived hydrologic attributes used to describe the spatial distribution of soil moisture. Areas on the landscape with high TWI values, predicted to be wetter sites, tended to exist lower on the transects or farther away from the catchment divide. These lower positions on the transect tended to have upslope areas with a smaller proportion of bedrock-dominated zones (UAAb < 50 %) and a greater proportion of upslope volume of B horizon (>11 %).

Elemental depletion (τ) of Ca, Na, and Al, an index of weathering extent, was correlated to groundwater metrics and topographic attributes. Elemental depletion was strongly correlated with saturation frequency ($r_s < -0.71$, $p < 0.05$) (Fig. 7, Fig. 3). Elemental depletion of Mg was not significantly correlated with any groundwater metrics and was

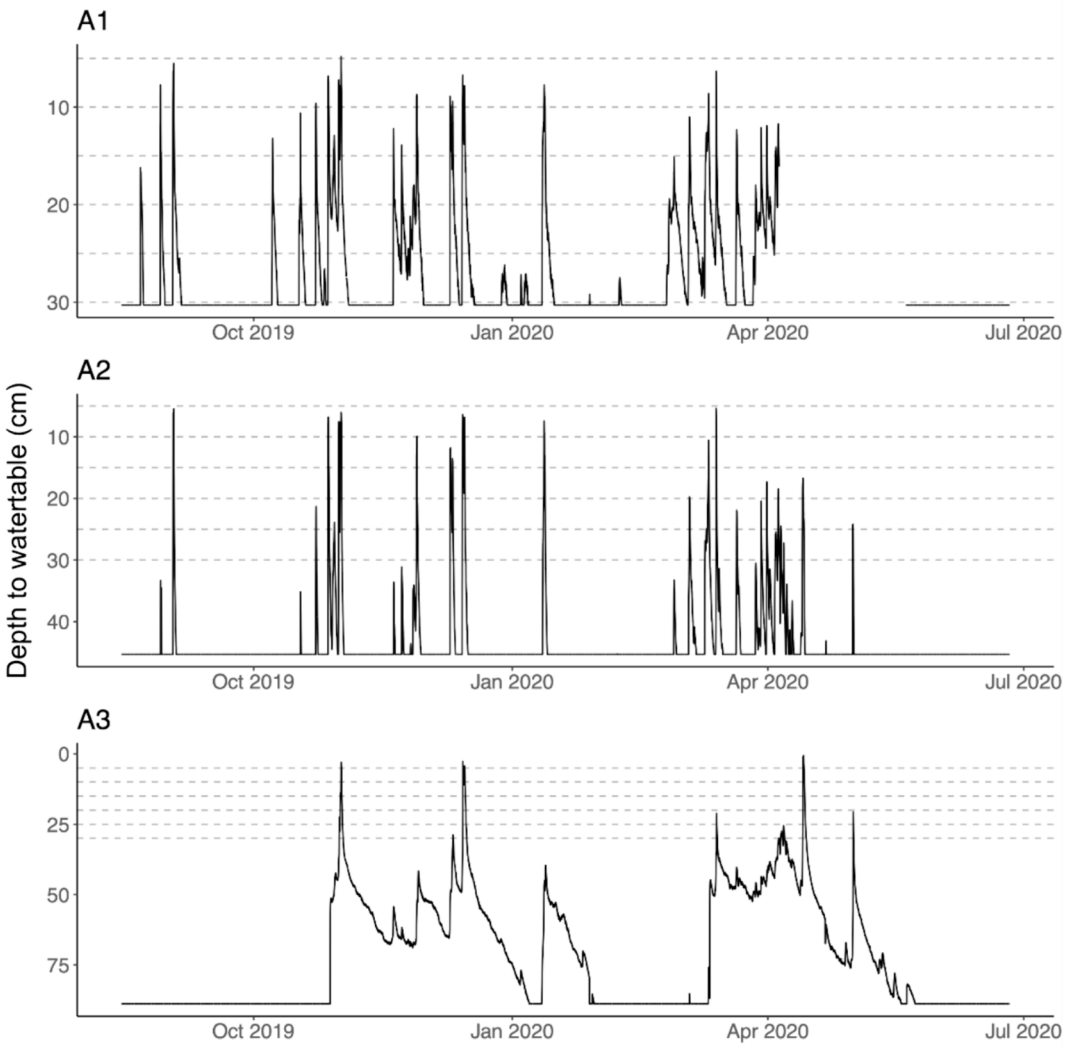

Fig. 5. Time series water level recording depths for all water level logging wells that were co-located with resins along transect A (hillslope positions 1–3) during the resin deployment period of one year, from August 2019–2020. All water levels are expressed as depth in centimeters from the soil surface. Steady water levels indicate the absence of the transient water table at the monitoring depth during that time, whereas the lack of a line (blank) indicates missing data due to logger errors. Dashed gray lines indicate the depths for which saturation frequency and duration were calculated for each well.

only negatively correlated with upslope drainage properties UAAb, PLAN, and CONVERGE ($r_s > -0.77$, $p < 0.05$).

We also examined relationships between mean upslope drainage area attributes and hydrologic behavior for the larger well network (n = 43), including wells co-located with deployed resins (Fig. 8). Not only did many of these wells have longer consecutive water level data (1–5 yrs), but they also more spatially distributed across the landscape (Fig. 1) and the range in topographic properties was thus larger (Table 1). There were many correlations that were similar as for the resin-associated wells (Figs. 7 and 8). The number of annual saturation cycles increased with increasing elevation ($r_s = 0.45$, $p < 0.01$). Saturation cycles were negatively correlated with mean upslope drainage area TWI ($r_s = -0.55$, $p < 0.01$) and flow accumulation ($r_s = -0.51$, $p < 0.01$). However, there were some notable contrasts between the strength and significance of correlation between saturation duration and topographic attributes between the two different Spearman analyses. For example, saturation duration calculated at the nine wells co-located with resins was not significantly correlated with many of the topographic attributes (Fig. 7). It did, however, positively correlate with how far it was from the catchment outlet (DISTOUT). In comparison, the analysis that included all wells throughout the catchment (n = 43), saturation duration was significantly correlated with several topographic properties (e.g., slope, topographic convergence, TWI).

4. Discussion

4.1. The role of catchment structure on shallow subsurface flow

Shallow groundwater metrics across Watershed 3 (n = 43) were strongly and significantly correlated with topography (Fig. 8). Results suggest that in a high relief catchment with well-drained soil, hydrodynamic behavior in the shallow soil zone (e.g., response depth, fluctuations, persistence) is influenced by both the local topographic setting and subsurface structure of the upslope drainage area.

Topographic wetness indices quantify the influence of topography on soil hydrology. In steep, forested watersheds it has been used to describe the spatial distribution of soil moisture, groundwater responses, the presence of wetlands, and soil development (e.g., Gillin et al., 2015; Grabs et al., 2009; Lidberg et al., 2020; Seibert et al., 2007; Seibert and McGlynn, 2007; Thompson and Moore, 1996). The upslope mean of topographic wetness index (TWI) using downslope index was the most important topographic variable for describing the spatial variability of saturation frequency ($r_s = -0.74$, $p < 0.01$), which was the number of times the water table rose and receded from the shallow portion of the

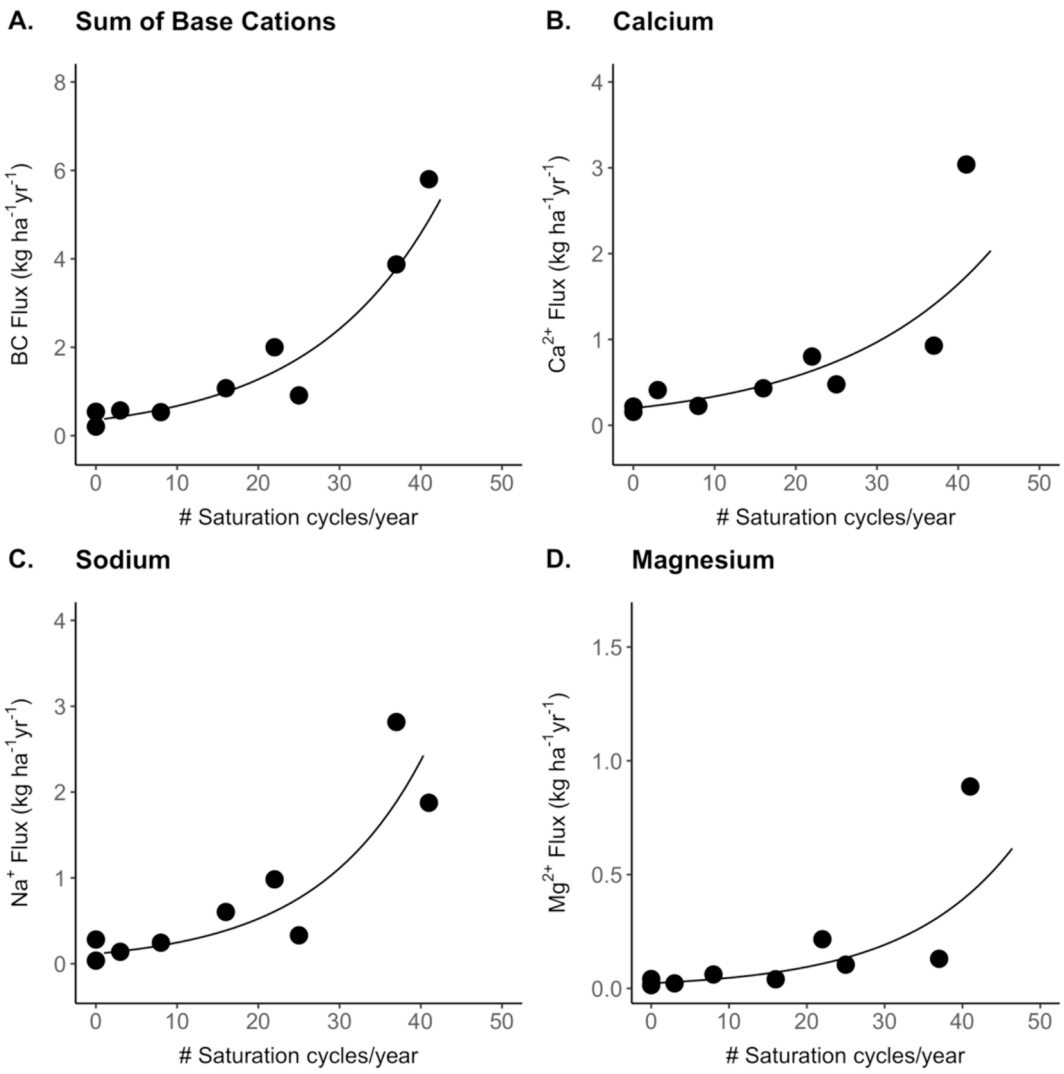

Fig. 6. Relationships and fitted exponential fits between measured base cation fluxes (kg ha^{-1} yr^{-1}) and saturation frequency at 20 cm, which is the number of times the water table reached and receded from 20 cm depth from the soil surface (cycles/year) during the resin deployment period. Saturation frequency was the strongest groundwater metric predictor variable of total base cation fluxes (see Fig. S7).

soil profile. As pointed out by Hjerdt et al. (2004), TWI calculated with the downslope index is less sensitive to irregular surface slope changes and better describes groundwater gradients. In general, soils with the highest annual saturation frequency occurred in ridge areas and had the lowest TWI values. TWI was highest in downslope positions closer to streams, where water levels were less dynamic (e.g., persistently wet). The strong and negative relationship between TWI and saturation frequency highlights the value of using TWI to describe the drainage efficiency of soils rather than the tendency to saturate. Annual saturation frequency was also strongly and positively related to slope convergence, planar slope curvature, and the proportion of bedrock outcrops in the upslope accumulated area (UAAb; $r_s > 0.54$). Numerous studies have shown that spatial extent and timing of soil saturation is influenced by the slope shape, as water is routed towards convergent points on the landscape (e.g., Kirkby and Chorley, 1967; Anderson and Burt, 1978; Hutchinson and Moore, 2000; Gevaert et al., 2014; Rinderer et al., 2014).

Observed spatial variations in saturation frequency in soils across the catchment indicate that local water table behavior was regulated by local slope and soil depth characteristics and the hydrologic properties of the upslope draining soils. Saturation frequency was greatest in shallow mineral soils nearest bedrock outcrops along ridges, where the transient water table would frequently and rapidly form near the soil surface and recede in response to storm events. During storm events, the water storage capacity of the thin and highly conductive organic soils surrounding the bedrock outcrops can easily be exceeded. The contribution of upslope water enhances the magnitude of water level rise in mineral soils. As the water table reaches near surface toward the organic (O) horizons, the lateral hydraulic gradient increases, and water is readily drained downslope by gravitational forces (Anderson and Burt, 1978). These processes together explain the frequent and rapid rise and recession of the water table in shallow mineral soils (e.g., high saturation frequency).

For this catchment, saturation frequency might be a groundwater metric that represents the propensity for lateral flow to dominate the hydrologic flux within soils versus vertical water percolation. Our data for Watershed 3 suggest that saturation frequency at 20 cm reflects a characteristic depth that best captures water table fluctuation variability and rapid wet up and drainage processes. Below 20 cm, fluctuations in the water table appear too similar (persistent water table) and any water table rise above 20 cm may have been too infrequent. This depth could also represent the average depth of the organic (O) horizon across the catchment, which is extremely permeable and could act as a preferential flow pathway routing water downslope rapidly. Saturation frequency was only calculated to 30 cm, which was approximately the depth of the shallowest well (A1; Fig. 5), so that comparisons between shallow soil

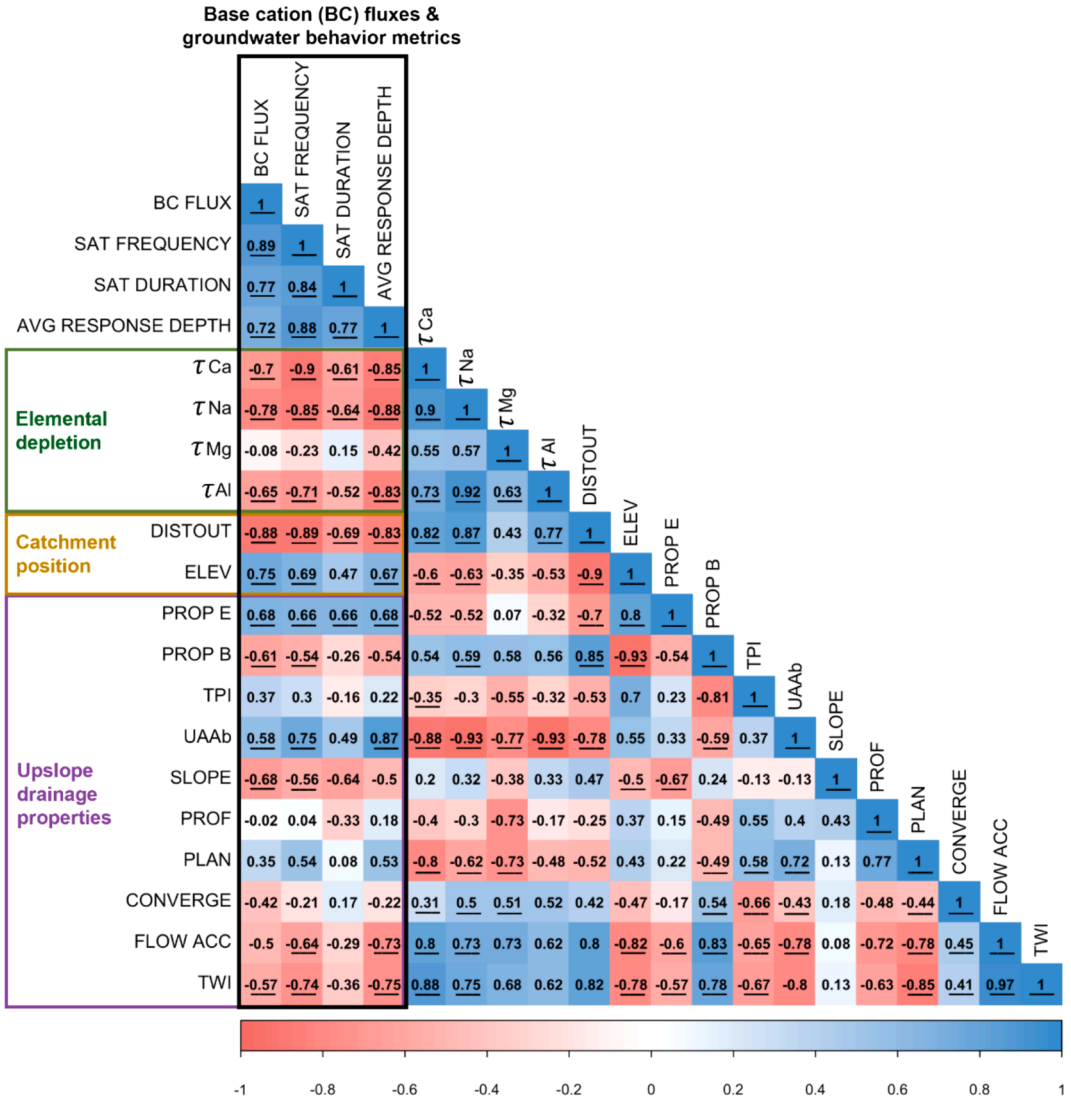

Fig. 7. Spearman correlation matrix for base cation fluxes, groundwater behavior metrics for wells near resins, elemental depletion of soil profiles, and catchment attributes for resin locations (see Fig. 1, purple boxed region). Underlined correlation values are statistically significant ($p < 0.05$) and the direction of the relationship as negative (red) or positive (blue). Abbreviations are for total base cation flux (BC FLUX), the number of saturation cycles (SAT CYCLES), duration of saturation (SAT DUR), mean water table response depth (MEAN), tau values (τ), distance to catchment outlet (DISTOUT), local elevation (ELEV), and mean upslope drainage area values for gradient (SLOPE), hillslope planar curvature (PLAN), hillslope profile curvature (PROF), convergence (CONVERGE), upslope flow accumulation (UAA), topographic wetness index (TWI), topographic position index, window size 100 m (TPI), and upslope accumulated area weighted by proportion with bedrock outcrop areas (UAAb).

water table fluctuations could be directly compared across the catchment.

In riparian areas near streams, where the solum is thicker and water storage capacity is greater, the average water table rise was much deeper in the soil profile and rarely rose into the B horizon. In this catchment, hydraulic conductivity is orders of magnitude lower in the C horizons compared to the solum above (Benton et al., 2022), which indicates that water drainage in the lower portions of the soil profile is much slower than when the water tables reach more conductive shallow soil horizons. While this work focuses on saturated soil conditions (e.g., when a water table exists), work by Gannon et al. (2017), showed that lateral flow also dominated in unsaturated conditions in shallow soils closer the bedrock outcrops, compared deeper soils near streams.

4.2. *Hydrologic flushing as a mechanism for base cation generation and transport*

Results from this study show that soil saturation frequency was the most important hydrologic variable for predicting base cation fluxes at a location (Fig. 7; Fig S7). High saturation frequency of soils near ridges is indicative of the dominance of lateral flow through the shallow soil zone in these portions of the catchment. Patterns in base cation fluxes likely reflect the spatial variation in soil hydrology, which regulates base cation generation, mobilization, and translocation.

Soil release of cations from desorption off the soil exchange complex could contribute to flux patterns during periods of rapid flushing, since ion exchange can occur at a rate of seconds to days, compared to slower mineral weathering rates (Brantley et al., 2008). At HBEF, clay content in soils is low, and exchangeable cation pools are related to carbon content in the Oa, Bh, and Bhs horizons (Dittman et al., 2007), with exchangeable Ca concentrations being orders of magnitude higher than Mg, Na, and K (Bailey, 2020) Bower et al. 2023b; Johnson et al., 1991a; b; Likens et al. 1998). While patterns of Ca fluxes (0.2 – 3.0 kg ha^{-1} yr^{-1}) could be influenced by cation exchange processes, they would not explain comparable Na fluxes (up to 2.8 kg ha^{-1} yr^{-1}). Na is not a major constituent of atmospheric deposition or secondary soil products (e.g.,

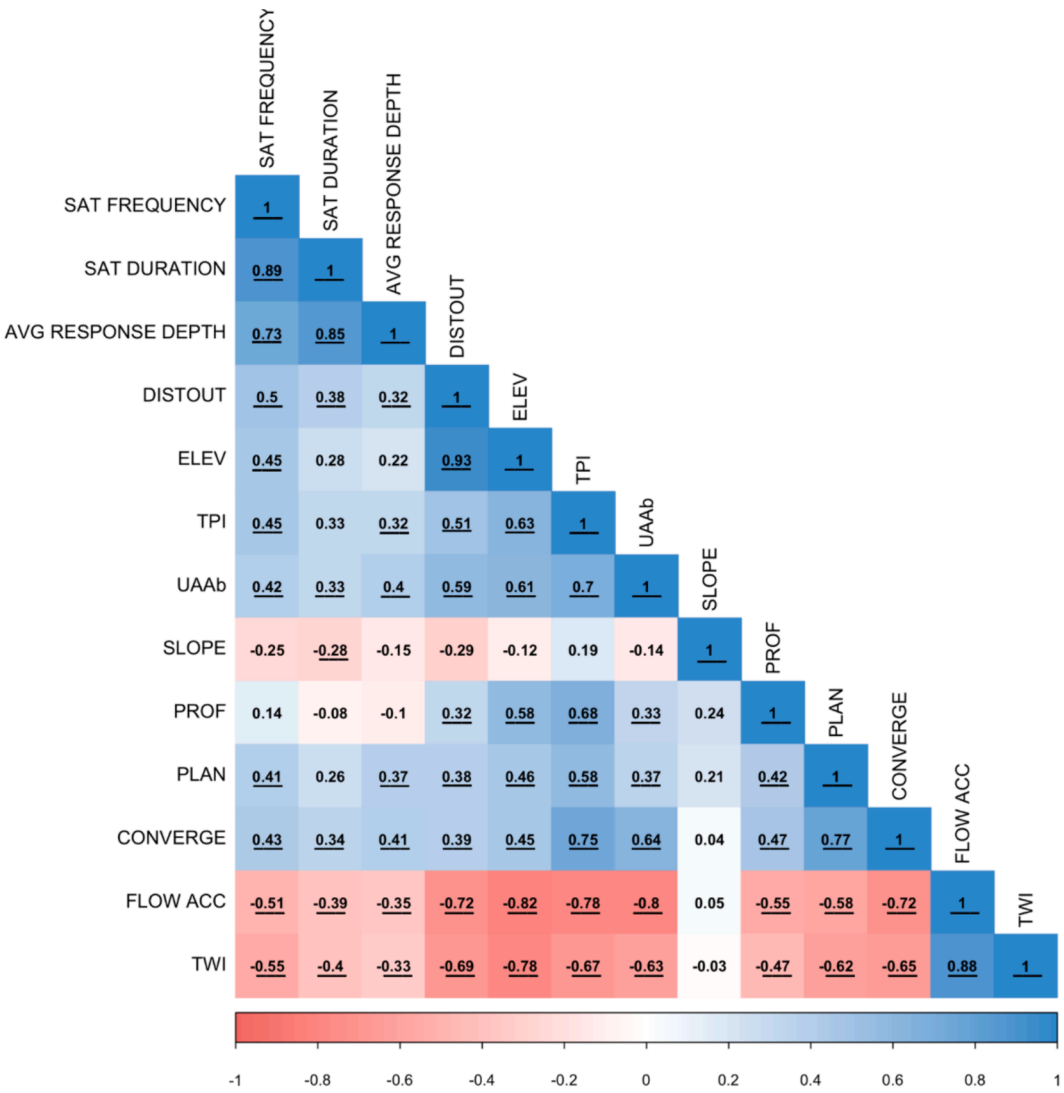

Fig. 8. Spearman correlation matrix between soil saturation metrics and catchment attributes for the entire Watershed 3 well network (n = 43; Fig. 1 white and purple dots). Underlined correlation values indicate the significance of the correlation ($p < 0.05$) and the direction of the relationship as negative (red) or positive (blue). Abbreviations are for total base cation flux (BC FLUX), the number of saturation cycles (SAT CYCLES), duration of saturation (SAT DUR), mean water table response depth (MEAN), distance to catchment outlet (DISTOUT), local elevation (ELEV), and mean upslope drainage area values for gradient (SLOPE), hillslope planar curvature (PLAN), hillslope profile curvature (PROF), convergence (CONVERGE), upslope flow accumulation (UAA), topographic wetness index (TWI), topographic position index (TPI), and upslope accumulated area weighted by proportion of area weighted by bedrock (UAAb).

Fe-, Al-oxides), and minimally participates in biologic cycling and exchange processes. For this reason, Na is often a useful conservative tracer for measuring mineral weathering fluxes, particularly from the dissolution of plagioclase (Bailey, 2020).

Repeated hydrologic flushing of the soil profile (high saturation frequency) could promote conditions that favor mineral dissolution reactions. As reaction products are flushed out of pore spaces, solute concentrations are lowered, and dissolution is favored by thermodynamic disequilibria (Benettin et al., 2015; Maher, 2011). Soils in mid and lower backslope positions were saturated for longer durations of time, although were less frequently flushed higher in the soil profile (low saturation frequency; Fig. 5, Fig. S5, S6), and had smaller base cation fluxes than soils near the ridges. These results suggest that the presence of longer or isolated flow paths may result in transport-limited weathering reactions if the soil solution is not often pushed away from chemical equilibrium. In a study by Clow and Drever (1996), increases in catchment chemical fluxes were attributed to episodic saturation during high flow events, inferring that the hydrologic flushing of the soil matrix and micropores increased chemical weathering rates. The importance of the flushing frequency mechanism, which assumes that greater volumes of water flowing though soil results in the leaching of a greater mass of solutes, has been suggested to explain varying patterns in subsurface flow chemistry, such as base cation concentrations (Burns et al., 1998), DOC (Boyer et al., 1997), and NO_3^- (Welsch et al., 2001). In the Panola Mountain Watershed in Georgia, Burns et al. (1998) found that water draining from a hillslope with more subsurface flow produced had lower base cation concentrations, thought to be contributed by historical soil flushing and the loss of base cations available for leaching. However, this hypothesis is complicated by the significant contribution of pipe flow to total subsurface flow in the Panola Mountain Watershed (Tromp-van Meerveld and McDonnell, 2006), which can bypass the soil matrix and affect soil water chemistry.

Base cation fluxes were strongly correlated with the proportion of bedrock outcrops and associated shallow organic soils in upslope drainage areas (UAAb; Fig. 7). Shallow groundwater and adjacent stream chemistry in bedrock-controlled areas of Watershed 3 are characterized by low pH values and high concentrations of DOC (Bailey et al., 2019; Zimmer et al., 2013). Bailey et al., (2019) suggests that the

translocation of upslope-generated organic acids is likely neutralized by the dissolution of silicate minerals in soil water draining from bedrock-controlled regions. Experimental studies have shown that plagioclase weathering accelerates with increasing acidity (e.g., Blum and Stillings, 1995; Welch and Ullman, 1996). The chemical dissolution of plagioclase is a primary source of Ca and Na, due to its high abundance and solubility, and is known to dominate weathering fluxes at HBEF (Bailey, 2020; Bailey 2003; Blum and Stillings, 1995; Bower et al., 2023a). Our measured annual fluxes associated with shallow subsurface flow for Ca and Na were on average much higher than Mg (Fig. 4), which likely reflects the lower abundance of and weathering contributions to the soil solution from Mg-bearing minerals, including biotite, chlorite, and hornblende (Bower et al., 2023a; Hyman et al., 1998).

Soil profiles where saturation frequency was highest (e.g., hillslope position 1 for transects A and B) had the highest estimate of base cation fluxes (Fig. 6) and were also most elementally depleted in Ca, Na, and Al (Fig. 3; Fig. S4). These spatial relationships could indicate that present day base cation fluxes represent spatial differences in the rates of chemical weathering and translocation. The loss of Ca, Na and Al from the dissolution of plagioclase would agree with the observed higher contribution of Ca and Na fluxes to the overall total base cation flux and the extent of depletion of these elements within the soil profiles in this study compared to Mg (Fig. 4, Fig. 3, Fig. S4). Our findings of high base cation fluxes and mineral depletion in locations where the transient water table often rises and recedes to the shallow portions of the profile aligns with the soil morphology observed at each location. Here, soil profiles are dominated by thick E-horizons above shallow bedrock. Eluvial horizons carry a physiochemical memory of long-term elemental weathering loss, and represent past and present hydrologic conditions (Lin, 2011).

There was a positive correlation between cation fluxes and elevation (Fig. 6); however, bulk precipitation chemistry at HBEF has shown no elevational gradient for Ca, Na, or Mg deposition, thus we expect precipitation to contribute minimally toward observed elevational flux trends (Likens et al., 1967). Upper elevations of this watershed are dominated by coniferous tree species, which have lower Ca and Mg concentrations in plant tissue than deciduous species in lower elevations (Arthur et al., 1999; Likens and Bormann, 1970; Likens et al., 1998). As a result, less of these elements are recycled back to soils, which is reflected by a decrease in exchangeable and organic matter Ca and Mg pools at higher elevations. Therefore, we expect Ca and Mg fluxes from the mineralization of organic matter or throughfall to be smaller at the top of the catchment, where measured fluxes of these elements were found to be greatest.

In a nearby catchment at HBEF, Nezat et al. (2004) provided similar evidence of intra-catchment spatial variability of chemical weathering. They determined that weathering rates were greatest in higher elevations of the catchment, attributed to increased contributions of organic acidity from conifers in shallow organic soils near ridges. Frequent flushing of acidic waters, transported with subsurface flow, is the possible agent behind enhanced weathering rates at locations where our observed present-day estimations of annual base cation fluxes are greatest and where more extensive long-term weathering has taken place (high depletion values). Our results show that base cation fluxes within Watershed 3 are highly variable within the shallow soil zone. And furthermore, they are highly dependent on shallow groundwater behavior throughout the catchment.

A notable exception to our observed trends between elemental loss and estimated base cation fluxes was for soil profile C1, which had only a thin E-horizon (<10 cm; Fig. 3), and the lowest estimate for all base cation fluxes (Fig. 4). A small mineral–water contact area with the sandy E horizon because of the small mineral soil volume upslope of this site could account for the small fluxes. While a mineral E-horizon was present directly on top of bedrock, the soil profile was, by depth ~85 % organic (Oi, Oe, Oa). Organic horizons are typically extremely porous and can rapidly transmit water (e.g., Deeks et al., 2004), which also could have prevented the formation of a water table due to such high saturated hydraulic conductivity.

4.3. Implications of solute flux heterogeneity in the shallow soil zone

The contribution of shallow soil to catchment export of base cations is often considered low, as shallow groundwater is often relatively dilute in cation concentrations compared to deeper groundwater sources (Bailey et al., 2023). However, our flux estimations were as high as 5.8 kg ha^{-1} yr^{-1} (Fig. 4). For context, a 10-year average base cation flux (sum of Ca, Na, Mg) at the Watershed 3 outlet is approximately 16 kg ha^{-1} yr^{-1}, meaning that shallow subsurface flow could represent up to ~38 % of the total catchment flux (HBWatER, 2021). Furthermore, the highest estimation of base cation fluxes were in soil types that only represent ~10 % of the total catchment area (Gillin et al., 2015). This underscores the importance of quantifying the spatial relationships between soils and their saturation dynamics, even within a single catchment, to make meaningful predictions of catchment export under varying hydrologic conditions.

At HBEF, the draining of acidic waters by subsurface flow is a major process impacting soil formation (Bailey et al., 2014; Bailey et al., 2019). Differences in the magnitude and direction of the hydrologic flux in the shallow soil zone (lateral flow vs. vertical percolation) results in two distinct modes of podzolization as evident by soil morphology and the spatial variation of soil organometallic complexes (Bourgault et al., 2017; Bourgault et al., 2015). Near bedrock outcrops, where lateral flow dominates the hydrologic flux, soils show distinct patterns of eluviation (loss of primary minerals) and downslope illuviation (accumulation of secondary minerals, i.e., spodic materials) along flow pathways. Work by Bower et al., (2023a) found that podzols formed through lateral podzolization processes are up to four times more depleted in plagioclase-bound elements than those formed through vertical podzolization processes. Our work suggests that base cations transported by subsurface flow could be, at least in part, sourced through these weathering reactions within the shallow soil zone.

Putting base cation generation into a hydrological framework is important for understanding not only the “hot spots” of mineral weathering on the landscape (bedrock-controlled regions) but also the “hot moments” where lateral subsurface flushing might enhance intra-catchment weathering rates. During larger storm events, stream networks expand up hillslopes and catchment hydrologic connectivity increases, therefore it could be expected that the transport of solutes from upland soils to streams is also enhanced (Brown et al., 1999; Detty and McGuire, 2010; Hornberger et al., 1994; Jencso et al. 2009).

5. Conclusions

We found that soil base cation fluxes (Ca, Na, and Mg) were not uniform along hillslopes. Fluxes ranged from 0.2 to 5.8 kg ha^{-1} yr^{-1} and varied greatly across small spatial scales (10 s of meters). Base cation generation and transport through the shallow soil zone are often considered negligible to overall catchment solute export, and few studies have shown how base cation fluxes via subsurface flow might vary spatially. Base cation fluxes were greatest at the top of the catchment near ridges and bedrock outcrops. Fluxes were positively and significantly correlated with elemental depletion of soil profiles in Ca, Na, and Al, which are the major constituents of plagioclase, a dominant parent mineral in this region. These portions of the landscape experience the highest number of soil saturation cycles (saturation frequency) within the shallow portion of the soil profile, which represents the frequent formation of a shallow transient water table that quickly drains downslope following storm events. Additionally, this work demonstrates the significant relationships between catchment topographic attributes and metrics of shallow groundwater behavior, which could be useful for predicting where lateral subsurface flow might dominate the hydrologic flux across similar landscapes.

To our knowledge, these types of time-integrated in situ measurements of annual solute fluxes associated with shallow subsurface flow has not been presented before. Our findings draw connections in how shallow subsurface flow might regulate the spatial patterns of base cations released from mineral weathering processes. The systematic variation in shallow groundwater dynamics with soil base cation fluxes underscores the influential role that catchment structure has on spatial patterns of solute generation and transport. We propose that the frequent flushing of water draining from bedrock outcrop areas of the landscape enhances the chemical dissolution of primary minerals along lateral flow paths. It is evident from this work that base cation fluxes associated with shallow subsurface flow may warrant further investigation, especially in steep, forested landscapes. While this study focused on a year-long integration of mass fluxes in upland soils of the catchment, future research could explore variations in fluxes between storm event magnitudes and/or in riparian areas closer to streams. Additionally, other studies could examine the impact of other soil chemical properties (e.g., soil exchange capacity) in conjunction with hydrologic interactions on the spatial distribution of elemental fluxes. Because the studied forest has been perturbed by forest harvest and chronic acid deposition over the last century, these fluxes are representative of dynamic, recovering ecosystems.

CRediT authorship contribution statement

Amanda Pennino: Writing – review & editing, Writing – original draft, Visualization, Validation, Project administration, Methodology, Investigation, Formal analysis, Data curation, Conceptualization. **Brian D. Strahm:** Writing – review & editing, Supervision, Resources, Methodology, Funding acquisition, Conceptualization. **Kevin J. McGuire:** Writing – review & editing, Supervision, Resources, Project administration, Methodology, Funding acquisition, Conceptualization. **Jennifer A. Bower:** Writing – review & editing, Visualization, Methodology, Investigation, Formal analysis, Data curation, Conceptualization. **Scott W. Bailey:** Writing – review & editing, Supervision, Resources, Project administration, Methodology, Investigation, Funding acquisition, Data curation, Conceptualization. **Madeline E. Schreiber:** Writing – review & editing, Supervision, Project administration, Investigation, Funding acquisition, Conceptualization. **Donald S. Ross:** Writing – review & editing, Supervision, Resources, Project administration, Investigation, Funding acquisition, Conceptualization. **Stephanie A. Duston:** Writing – review & editing, Methodology, Investigation, Data curation, Conceptualization. **Joshua R. Benton:** Writing – review & editing, Methodology, Investigation, Data curation, Conceptualization.

Declaration of competing interest

The authors declare the following financial interests/personal relationships which may be considered as potential competing interests: Amanda Pennino reports financial support was provided by National Science Foundation. Amanda Pennino reports financial support was provided by International Long-Term Ecological Research Network. Amanda Pennino reports financial support was provided by Virginia Tech Global Change Center. Amanda Pennino reports a relationship with USDA-NRCS National Soil Survey Center that includes: employment, non-financial support, speaking and lecture fees, and travel reimbursement. If there are other authors, they declare that they have no known competing financial interests or personal relationships that could have appeared to influence the work reported in this paper.

Data availability

Data will be made available on request.

Acknowledgement

We thank Delaney Peterson, Kara Crawford, Kaitlyn Hogarth, David Mitchem, and Jeffrey Parks for their help with lab analyses, and Delaney Peterson and Nathaniel Rasnake for their aid in the field. Hubbard Brook Experimental Forest is managed by the USDA Forest Service, Northern Research Station, Madison, WI. We thank Katy Dynarski and Shawn Salley for their constructive feedback which helped improve the manuscript.

Funding

This work was supported by the National Science Foundation Geobiology and Low Temperature Geochemistry Program [EAR 1643327; 2018] and Long-Term Ecological Research Network, LTER [DEB 1637685; 2016]. Additional support was provided by the Global Change Center at Virginia Tech and the Edna Bailey Sussman Foundation.

Appendix A. Supplementary data

Supplementary data to this article can be found online at https://doi.org/10.1016/j.geoderma.2024.117045.

References

Anderson, M.G., Burt, T.P., 1978. The role of topography in controlling throughflow generation. Earth Surf. Process. 3 (4), 331–344. https://doi.org/10.1002/esp.3290030402.

Annable, M.D., Hatfield, K., Cho, J., Klammler, H., Parker, C.L., Cherry, J.A., Rao, P.S.C., 2005. Field-scale evaluation of the passive flux meter for simultaneous measurement of groundwater and contaminant fluxes. Environ. Sci. Tech. 39 (18), 7194–7201.

Arthur, M.A., Siccama, T.G., Yanai, R.D., 1999. Calcium and magnesium in wood of northern hardwood forest species: relations to site characteristics. Can. J. For. Res. 29, 339–346.

Bailey, S.W., Brousseau, P.A., McGuire, K.J., Ross, D.S., 2014. Influence of landscape position and transient water table on soil development and carbon distribution in a steep, headwater catchment. Geoderma 226–227, 279–289. https://doi.org/10.1016/j.geoderma.2014.02.017.

Bailey, S.W., J.P. Gannon, K.J. McGuire, L.H. Pardo, and A.M. Pennino. 2023. Hubbard Brook Experimental Forest: Watershed 3 Subsurface Water Chemistry ver 3. Environmental Data Initiative. https://doi.org/10.6073/pasta/d82538ddccb6b97906050e6e45cb816a (Accessed 2023-12-15).

Bailey, S.W., McGuire, K.J., Ross, D.S., Green, M.B., Fraser, O.L., 2019. Mineral weathering and podzolization control acid neutralization and streamwater chemistry gradients in upland glaciated catchments, Northeastern United States. Front. Earth Sci. 7 (63). https://doi.org/10.3389/feart.2019.00063.

Bailey, A.S., 2003. Hydrometeorological Database for Hubbard Brook Experimental Forest, 1955-2000 (Vol. 305). US Department of Agriculture, Forest Service, Northeastern Research Station.

Bailey, S.W. 2020. Tracking the fate of plagioclase weathering products: pedogenic and human influences. Biogeochemical Cycles: Ecological Drivers and Environmental Impact, pp.151-162.

Bailey, S.W., Gannon, J.B., McGuire, K.J., Green, M.B., Pennino, A.M., 2024, Hubbard Brook Experimental Forest: Watershed 3 well water level recordings, 2007 - ongoing ver 4. Environmental Data Initiative. https://doi.org/10.6073/pasta/210b60a3d2f5ee2bb2635ee2fb33b637 (Accessed 2024-09-23).

Bazemore, D.E., Eshleman, K.N., Hollenbeck, K.J., 1994. The role of soil water in stormflow generation in a forested headwater catchment: synthesis of natural tracer and hydrometric evidence. J. Hydrol. 162 (1–2), 47–75.

Benton, J.R., McGuire, K.J., Schreiber, M.E., 2022. Subsurface permeability contrasts control shallow groundwater flow dynamics in the critical zone of a glaciated, headwater catchment. Hydrol. Process. 36 (9), e14672.

Blum, A.E., L.L. Stillings. 1995. "Chapter 7. FELDSPAR DISSOLUTION KINETICS." In Chemical Weathering Rates of Silicate Minerals, edited by Arthur F. White and Susan L. Brantley, 291–352. De Gruyter. https://doi.org/10.1515/9781501509650-009.

Beven, K., Germann, P., 1982. Macropores and water flow in soils. Water resources research 18 (5), 1311–1325.

Bourgault, R.R., Ross, D.S., Bailey, S.W., 2015. Chemical and morphological distinctions between vertical and lateral podzolization at Hubbard brook. Soil Sci. Soc. Am. J. 79 (2), 428–439. https://doi.org/10.2136/sssaj2014.05.0190.

Bourgault, R.R., Ross, D.S., Bailey, S.W., Bullen, T.D., McGuire, K.J., Gannon, J.P., 2017. Redistribution of soil metals and organic carbon via lateral flowpaths at the catchment scale in a glaciated upland setting. Geoderma 307, 238–252. https://doi.org/10.1016/j.geoderma.2017.05.039.

Bower, J.A., Pennino, A.M., McGuire, K.J. 2023b. Hubbard Brook Experimental Forest: Watershed 3 Lateral Weathering Soil Chemistry ver 1. Environmental Data Initiative. https://doi.org/10.6073/pasta/7348ab7d97a765b612687ba547a7aa47 (Accessed 2024-01-05).

Bower, J.A., Pennino, A.M., Bailey, S.W., McGuire, K.J., Duston, S.A. 2023c. Hubbard Brook Experimental Forest: Watershed 3 Lateral Weathering Pedon Descriptions ver 3. Environmental Data Initiative. https://doi.org/10.6073/pasta/ed5326149d2fea068d6c8d4d550718ec (Accessed 2024-01-10).
Bower, J.A., Ross, D.S., Bailey, S.W., Pennino, A.M., Jercinovic, M.J., McGuire, K.J., Strahm, B.D., Schreiber, M.E., 2023a. Development of a lateral topographic weathering gradient in temperate forested podzols. Geoderma 439, 116677.
Boyer, E.W., Hornberger, G.M., Bencala, K.E., McKnight, D.M., 1997. Response characteristics of DOC flushing in an alpine catchment. Hydrol. Process. 11 (12), 1635–1647.
Bracken, L.J., Croke, J., 2007. The concept of hydrological connectivity and its contribution to understanding runoff-dominated geomorphic systems. Hydrol. Process. 21 (13), 1749–1763. https://doi.org/10.1002/hyp.6313.
Brantley, S.L., Kubicki, J.D., White, A.F. (Eds.), 2008. Kinetics of Water-Rock Interaction. Springer Verlag, New York.
Brimhall, G.H., Dietrich, W.E., 1987. Constitutive mass balance relations between chemical composition, volume, density, porosity, and strain in metasomatic hydrochemical systems: results on weathering and pedogenesis. Geochim. Cosmochim. Acta 51 (3), 567–587.
Brown, V.A., McDonnell, J.J., Burns, D.A., Kendall, C., 1999. The role of event water, a rapid shallow flow component, and catchment size in summer stormflow. J. Hydrol. 217 (3), 171–190. https://doi.org/10.1016/S0022-1694(98)00247-9.
Burns, D.A., Hooper, R.P., McDonnell, J.J., Freer, J.E., Kendall, C., Beven, K., 1998. Base cation concentrations in subsurface flow from a forested hillslope: the role of flushing frequency. Water Resour. Res. 34 (12), 3535–3544.
Burns, D.A., McDonnell, J.J., Hooper, R.P., Peters, N.E., Freer, J.E., Kendall, C., Beven, K., 2001. Quantifying contributions to storm runoff through end-member mixing analysis and hydrologic measurements at the Panola Mountain Research Watershed (Georgia, USA). Hydrological processes 15 (10), 1903–1924.
Buttle, J.M., 1994. Isotope hydrograph separations and rapid delivery of pre-event water from drainage basins. Prog. Phys. Geogr. 18 (1), 16–41.
Campbell, T.J., Hatfield, K., Klammler, H., Annable, M.D., Rao, P.S.C., 2006. Magnitude and directional measures of water and Cr (VI) fluxes by passive flux meter. Environ. Sci. Tech. 40 (20), 6392–6397.
Chifflard, P., Blume, T., Maerker, K., Hopp, L., van Meerveld, I., Graef, T., Gronz, O., Hartmann, A., Kohl, B., Martini, E., Reinhardt-Imjela, C., Reiss, M., Rinderer, M., Achleitner, S., 2019. How can we model subsurface stormflow at the catchment scale if we cannot measure it? Hydrol. Process. 2019 (33), 1378–1385. https://doi.org/10.1002/hyp.13407.
Christophersen, N., Hooper, R.P., 1992. Multivariate analysis of stream water chemical data: the use of principal components analysis for the end-member mixing problem. Water Resour. Res. 28 (1), 99–107.
Clow, D.W., Drever, J.I., 1996. Weathering rates as a function of flow through an alpine soil. Chem. Geol. 132 (1–4), 131–141. https://doi.org/10.1016/S0009-2541(96)00048-4.
de Jonge, H., Rothenberg, G., 2005. New device and method for flux-proportional sampling of mobile solutes in soil and groundwater. Environ. Sci. Tech. 39 (1), 274–282.
Deeks, L.K., Bengough, A.G., Low, D., Billett, M.F., Zhang, X., Crawford, J.W., Chessell, J. M., Young, I.M., 2004. Spatial variation of effective porosity and its implications for discharge in an upland headwater catchment in Scotland. J. Hydrol. 290 (3–4), 217–228.
Detty, J.M., McGuire, K.J., 2010. Topographic controls on shallow groundwater dynamics: implications of hydrologic connectivity between hillslopes and riparian zones in a till mantled catchment. Hydrol. Process. 24 (16), 2222–2236. https://doi.org/10.1002/hyp.7656.
Dittman, J.A., Driscoll, C.T., Groffman, P.M., Fahey, T.J., 2007. Dynamics of nitrogen and dissolved organic carbon at the Hubbard Brook Experimental Forest. Ecology 88 (5), 1153–1166.
Dixon, J.L., Chadwick, O.A., Vitousek, P.M., 2016. Climate-driven thresholds for chemical weathering in postglacial soils of New Zealand. J. Geophys. Res. Earth 121 (9), 1619–1634. https://doi.org/10.1002/2016JF003864.
Fraser, O., Bailey, S.W., Ducey, M.J., McGuire, K.J., 2020. Predictive modeling of bedrock outcrops and associated shallow soil in upland glaciated landscapes. Geoderma 376.
Fraser, O.L., McGuire, K.J., Bailey, S.W. 2022. Hubbard Brook Experimental Forest: 1 meter LiDAR-derived and Hydro-enforced Digital Elevation Models, 2012.
Fraser, O.L., Gannon, J.P., Bailey, S.W., McGuire, K.J. 2024. Hubbard Brook Experimental Forest: Soil type prediction raster files ver 2. Environmental Data Initiative. https://doi.org/10.6073/pasta/a000ef8c9274155b5b2b4bf9622ead23 (Accessed 2024-05-23).
Freer, J., McDonnell, J.J., Beven, K.J., Peters, N.E., Burns, D.A., Hooper, R.P., Aulenbach, B., Kendall, C., 2002. The role of bedrock topography on subsurface storm flow. Water Resour. Res. 38 (12), 5-1–5-16. https://doi.org/10.1029/2001WR000872.
Gannon, J.P., Bailey, S.W., McGuire, K.J., 2014. Organizing groundwater regimes and response thresholds by soils: a framework for understanding runoff generation in a headwater catchment. Water Resour. Res. 50 (11), 8403–8419.
Gannon, J.P., McGuire, K.J., Bailey, S.W., Bourgault, R.R., Ross, D.S., 2017. Lateral water flux in the unsaturated zone: a mechanism for the formation of spatial soil heterogeneity in a headwater catchment. Hydrol. Process. 31 (20), 3568–3579. https://doi.org/10.1002/hyp.11279.
Garrett, C., Vulava, V.M., Callahan, T.J., Jones, M.L., 2012. Groundwater–surface water interactions in a lowland watershed: source contribution to stream flow. Hydrological Processes 26 (21), 3195–3206.
Gevaert, A.I., Teuling, A.J., Uijlenhoet, R., DeLong, S.B., Huxman, T.E., Pangle, L.A., Breshears, D.D., Chorover, J., Pelletier, J.D., Saleska, S.R., Zeng, X., 2014. Hillslope-scale experiment demonstrates the role of convergence during two-step saturation. Hydrol. Earth Syst. Sci. 18 (9), 3681–3692.
Gillin, C.P., Bailey, S.W., McGuire, K.J., Gannon, J.P., 2015. Mapping of hydropedologic spatial patterns in a steep headwater catchment. Soil Sci. Soc. Am. J. 79 (2), 440–453. https://doi.org/10.2136/sssaj2014.05.0189.
Godsey, S.E., Kirchner, J.W., Clow, D.W., 2009. Concentration-discharge relationships reflect chemostatic characteristics of US catchments. Hydrol. Process. 23 (13), 1844–1864. https://doi.org/10.1002/hyp.7315.
Grabs, T., Seibert, J., Bishop, K., Laudon, H., 2009. Modeling spatial patterns of saturated areas: A comparison of the topographic wetness index and a dynamic distributed model. Journal of Hydrology 373 (1–2), 15–23.
Guisan, A., Weiss, S.B., Weiss, A.D., 1999. GLM versus CCA spatial modeling of plant species distribution. Plant Ecol. 143 (1), 107–122. https://doi.org/10.1023/A:1009841519580.
Hatfield, K., Annable, M., Cho, J., Rao, P.S.C., Klammler, H., 2004. A Direct passive method for measuring water and contaminant fluxes in porous media. J. Contam. Hydrol. 75 (3–4), 155–181. https://doi.org/10.1016/j.jconhyd.2004.06.005.
Hubbard Brook Watershed Ecosystem Record (HBWatER). 2021. Hubbard Brook Experimental Forest: Chemistry of Streamwater – Monthly Fluxes, Watershed 3, 1963 - present ver 17. Environmental Data Initiative. https://doi.org/10.6073/pasta/ea3bf94e20a93b0e43b1a28fd0e5a38a (Accessed 2023-12-05).
Hewlett, J.D., Hibbert, A.R., 1967. Factors affecting the response of small watersheds to precipitation in humid areas. Forest hydrology. In: Sopper, W.E., Lull, H.W. (Eds.), International Symposium on Forest Hydrology. Pergamon Press, Oxford, UK, pp. 275–290.
Hjerdt, K.N., McDonnell, J.J., Seibert, J., Rodhe, A., 2004. A new topographic index to quantify downslope controls on local drainage. Water Resour. Res. 40 (5).
Hooper, R.P., Christophersen, N., Peters, N.E., 1990. Modelling streamwater chemistry as a mixture of soil water end-members—An application to the Panola Mountain catchment, Georgia, USA. J. Hydrol. 116 (1–4), 321–343.
Hornberger, G.M., Bencala, K.E., McKnight, D.M., 1994. Hydrological controls on dissolved organic carbon during snowmelt in the Snake River near Montezuma, Colorado. Biogeochemistry 25 (3), 147–165. https://doi.org/10.1007/BF00024390.
Hutchinson, D.G., Moore, R.D., 2000. Throughflow variability on a forested hillslope underlain by compacted glacial till. Hydrol. Process. 14 (10), 1751–1766.
Hyman, M.E., Johnson, C.E., Bailey, S.W., Hornbeck, J.W., April, R.H., 1998. Chemical weathering and cation loss in a base-poor watershed. Geol. Soc. Am. Bull. 110 (1), 85–95.
Inamdar, S.P., Mitchell, M.J., 2006. Hydrologic and topographic controls on storm-event exports of dissolved organic carbon (DOC) and nitrate across catchment scales. Water Resour. Res. 42 (3).
Inamdar, S.P., Mitchell, M.J., 2007. Contributions of riparian and hillslope waters to storm runoff across multiple catchments and storm events in a glaciated forested watershed. J. Hydrol. 341 (1–2), 116–130.
Jackson, C.R., 1992. Hillslope infiltration and lateral downslope unsaturated flow. Water Resour. Res. 28 (9), 2533–2539.
Jankowski, M., 2014. The evidence of lateral podzolization in sandy soils of Northern Poland. Catena 112 (January), 139–147. https://doi.org/10.1016/j.catena.2013.03.013.
Jencso, K., McGlynn, B.L., Gooseff, M.N., Wondzell, S.M., Bencala, K.E., Marshall, L.A., 2009. Hydrologic connectivity between landscapes and streams: transferring reach- and plot-scale understanding to the catchment scale. Water Resour. Res. 45 (4). https://doi.org/10.1029/2008WR007225.
Johnson, C.E., Johnson, A.H., Siccama, T.G., 1991a. Whole-tree clear-cutting effects on exchangeable cations and soil acidity. Soil Sci. Soc. Am. J. 55 (2), 502–508.
Johnson, C.E., Johnson, A., Siccama, T., 1991b. Whole-tree clear-cutting effects on exchangeable cations and soil acidity. Soil Sci. Soc. Am. J. 55, 502–508.
Johnson, C.E., Driscoll, C.T., Siccama, T.G., Likens, G.E., 2000. Element fluxes and landscape position in a northern hardwood forest watershed ecosystem. Ecosystems 3 (2), 159–184. https://doi.org/10.1007/s100210000017.
Johnson, D.W., Verburg, P.S.J., Arnone, J.A., 2005. Soil extraction, ion exchange resin, and ion exchange membrane measures of soil mineral nitrogen during incubation of a tallgrass prairie soil. Soil Sci. Soc. Am. J. 69 (1), 260–265.
Kiewiet, L., Freyberg, J., van Meerveld, H.J., 2019. Spatiotemporal variability in hydrochemistry of shallow groundwater in a small pre-alpine catchment: the importance of landscape elements. Hydrol. Process. 33 (19), 2502–2522. https://doi.org/10.1002/hyp.13517.
Kim, H., Dietrich, W.E., Thurnhoffer, B.M., Bishop, J.K.B., Fung, I.Y., 2017. Controls on solute concentration-discharge relationships revealed by simultaneous hydrochemistry observations of hillslope runoff and stream flow: the importance of critical zone structure. Water Resour. Res. 53 (2), 1424–1443. https://doi.org/10.1002/2016WR019722.
Kirkby, M.J., Chorley, R.J., 1967. Throughflow, overland flow and erosion. Hydrological Sciences Journal 12 (3), 5–21.
Kjønaas, O.J., 1999. In situ efficiency of ion exchange resins in studies of nitrogen transformation. Soil Sci. Soc. Am. J. 63 (2), 399–409. https://doi.org/10.2136/sssaj1999.03615995006300020019x.
Klaus, J., Jackson, C.R., 2018. Interflow is not binary: a continuous shallow perched layer does not imply continuous connectivity. Water Resour. Res. 54 (9), 5921–5932.
Klaus, J., McDonnell, J.J., 2013. Hydrograph separation using stable isotopes: review and evaluation. J. Hydrol. 505, 47–64.
Knapp, J.L.A., von Freyberg, J., Studer, B., Kiewiet, L., Kirchner, J.W., 2020. Concentration-discharge relationships vary among hydrological events, reflecting

differences in event characteristics. Hydrol. Earth Syst. Sci. 24 (5), 2561–2576. https://doi.org/10.5194/hess-24-2561-2020.
Kowalenko, C.G., Babuin, D., 2014. Use of lithium metaborate to determine total phosphorus and other element concentrations in soil, plant, and related materials. Commun. Soil Sci. Plant Anal. 45 (1), 15–28.
Lawrence, G.B., Burns, D.A., Riva-Murray, K., 2016. A new look at liming as an approach to accelerate recovery from acidic deposition effects. Sci. Total Environ. 562, 35–46. https://doi.org/10.1016/j.scitotenv.2016.03.176.
Lehmann, J., Kaiser, K., Peter, I., 2001. Exchange resin cores for the estimation of nutrient fluxes in highly permeable tropical soil. J. Plant Nutr. Soil Sci. 164 (1), 57–64.
Li, L., Bao, C., Sullivan, P.L., Brantley, S., Shi, Y., Duffy, C., 2017. Understanding watershed hydrogeochemistry: 2. Synchronized hydrological and geochemical processes drive stream chemostatic behavior. Water Resour. Res. 53 (3), 2346–2367. https://doi.org/10.1002/2016WR018935.
Lidberg, W., Nilsson, M., Ågren, A., 2020. Using machine learning to generate high-resolution wet area maps for planning forest management: a study in a boreal forest landscape. Ambio 49 (2), 475–486.
Likens, G.E., Bormann, F.H., Johnson, N.M., Pierce, R.S., 1967. The Calcium, magnesium, potassium, and sodium budgets for a small forested ecosystem. Ecology 48 (5), 772–785. https://doi.org/10.2307/1933735.
Likens, G.E., Driscoll, C.T., Buso, D.C., 1996. Long-term effects of acid rain: response and recovery of a forest ecosystem. Science 272 (5259), 244–246.
Likens, G.E., Driscoll, C.T., Buso, D.C., Siccama, T.G., Johnson, C.E., Lovett, G.M., Fahey, T.J., et al., 1998. The biogeochemistry of calcium at hubbard brook. Biogeochemistry 41 (2), 89–173. https://doi.org/10.1023/A:1005984620681.
Lin, H., 2010. Earth's Critical Zone and hydropedology: concepts, characteristics, and advances. Hydrol. Earth Syst. Sci. 14 (1), 25–45.
Lin, H., 2011. Three principles of soil change and pedogenesis in time and space. Soil Science Society of America Journal 75 (6), 2049–2070.
Lin, H.S., Kogelmann, W., Walker, C., Bruns, M.A., 2006. Soil moisture patterns in a forested catchment: a hydropedological perspective. Geoderma 131 (3–4), 345–368.
Lindsay, J.B. 2014. The Whitebox Geospatial Analysis Tools Project and Open-Access GIS. Proceedings of the GIS Research UK 22nd Annual Conference.
Maher, K., 2010. The dependence of chemical weathering rates on fluid residence time. Earth Planet. Sci. Lett. 294 (1–2), 101–110.
Maher, K., 2011. The role of fluid residence time and topographic scales in determining chemical fluxes from landscapes. Earth Planet. Sci. Lett. 312 (1), 48–58. https://doi.org/10.1016/j.epsl.2011.09.040.
McGlynn, B.L., McDonnell, J.J., 2003. Role of discrete landscape units in controlling catchment dissolved organic carbon dynamics. Water Resour. Res. 39 (4). https://doi.org/10.1029/2002WR001525.
McGuire, K.J., McDonnell, J.J., Weiler, M., Kendall, C., McGlynn, B.L., Welker, J.M., Seibert, J., 2005. The role of topography on catchment-scale water residence time. Water Resour. Res. 41 (5). https://doi.org/10.1029/2004WR003657.
Musolff, A., Zhan, Q., Dupas, R., Minaudo, C., Fleckenstein, J.H., Rode, M., Dehaspe, J., Rinke, K., 2021. Spatial and temporal variability in concentration-discharge relationships at the event scale. Water Resour. Res. 57 (10). https://doi.org/10.1029/2020WR029442.
Nezat, C.A., Blum, J.D., Klaue, A., Johnson, C.E., Siccama, T.G., 2004. Influence of landscape position and vegetation on long-term weathering rates at the Hubbard brook experimental forest, New Hampshire, USA. Geochim. Cosmochim. Acta 68 (14), 3065–3078. https://doi.org/10.1016/j.gca.2004.01.021.
Park, S.J., Burt, T.P., 2002. Identification and characterization of pedogeomorphological processes on a hillslope. Soil Sci. Soc. Am. J. 66 (6), 1897–1910.
Pearce, A., Stewart, M.K., Sklash, M.G., 1986. Storm runoff generation in humid headwater catchments. 1. Where does the water come from? Water Resour. Res. 22 (8), 1263–1272.
Pennino, A.M., McGuire, K.J., Strahm, B.D., Bailey, S.W. 2023. Hubbard Brook Experimental Forest: Watershed 3 – One year of resin-extracted solutes from variably saturated soils ver 2. Environmental Data Initiative. https://doi.org/10.6073/pasta/60f964ffa4e180eb19ee9249219cfa4e (Accessed 2023-05-14).
Pinder, G.F., Jones, J.F., 1969. Determination of the ground-water component of peak discharge from the chemistry of total runoff. Water Resour. Res. 5 (2), 438–445.
R Core Team. 2021. R: A language and environment for statistical computing. R Foundation for Statistical Computing, Vienna, Austria. URL https://www.R-project.org/.
Rinderer, M., van Meerveld, H.J., Seibert, J., 2014. Topographic controls on shallow groundwater levels in a steep, prealpine catchment: when are the TWI assumptions valid? Water Resour. Res. 50 (7), 6067–6080.
RStudio Team, 2020. RStudio: Integrated Development for R. RStudio, PBC, Boston, MA http://www.rstudio.com/.
Schoeneberger, Philip J., Wysocki, D.A., Benham, E.C. 2012. Field Book for Describing and Sampling Soils. Government Printing Office.
Seibert, J., McGlynn, B.L., 2007. A new triangular multiple flow direction algorithm for computing upslope areas from gridded digital elevation models: a new triangular multiple-flow direction. Water Resour Res. 43 (4). https://doi.org/10.1029/2006WR005128.
Seibert, J., Stendahl, J., Sørensen, R., 2007. Topographical influences on soil properties in boreal forests. Geoderma 141 (1-2), 139–148.
Simonson, R.W., 1959. Outline of a generalized theory of soil genesis. Soil Sci. Soc. Am. J. 23 (2), 152–156.
Sommer, M., Halm, D., Weller, U., Zarei, M., Stahr, K., 2000. Lateral podzolization in a granite landscape. Soil Sci. Soc. Am. J. 64, 9.
Sommer, M., Halm, D., Geisinger, C., Andruschkewitsch, I., Zarei, M., Stahr, K., 2001. Lateral podzolization in a sandstone catchment. Geoderma 103 (3), 231–247. https://doi.org/10.1016/S0016-7061(01)00018-0.
Spearman, C., 1904. The proof and measurement of association between two things. Am. J. Psychol. 15, 72–101.
Soil Survey Staff. 2022. Keys to Soil Taxonomy, 13th edition. USDA Natural Resources Conservation Service.
Stewart, B., Shanley, J.B., Kirchner, J.W., Norris, D., Adler, T., Bristol, C., Harpold, A.A., Perdrial, J.N., Rizzo, D.M., Sterle, G., Underwood, K.L., 2022. Streams as mirrors: reading subsurface water chemistry from stream chemistry. Water Resour. Res. 58 (1) e2021WR029931.
Tetzlaff, D., Seibert, J., McGuire, K.J., Laudon, H., Burns, D.A., Dunn, S.M., Soulsby, C., 2009. How does landscape structure influence catchment transit time across different geomorphic provinces? Hydrol. Process. 23 (6), 945–953. https://doi.org/10.1002/hyp.7240.
Thompson, J.C., Moore, R.D., 1996. Relations between topography and water table depth in a shallow forest soil. Hydrol. Process. 10, 1513–1525.
Tokunaga, T.K., Tran, A.P., Wan, J., Dong, W., Newman, A.W., Beutler, C.A., Brown, W., Henderson, A.N., Williams, K.H., 2022. Quantifying subsurface flow and solute transport in a snowmelt-recharged Hillslope with multiyear water balance. Water Resour. Res. 58 (12) e2022WR032902.
Tromp-van Meerveld, H.J., McDonnell, J.J., 2006. Threshold relations in subsurface stormflow: 1. A 147-storm analysis of the Panola hillslope. Water Resour. Res. 42 (2).
Wang, L., Liu, H., 2006. An efficient method for identifying and filling surface depressions in digital elevation models for hydrologic analysis and modelling. Int. J. Geogr. Inf. Sci. 20 (2), 193–213.
Watmough, S.A., Aherne, J., Alewell, C., Arp, P., Bailey, S., Clair, T., Dillon, P., Duchesne, L., Eimers, C., Fernandez, I., Foster, N., 2005. Sulphate, nitrogen and base cation budgets at 21 forested catchments in Canada, the United States and Europe. Environmental monitoring and assessment 109, 1–36.
Weiler, M., McDonnell, J.J., van Meerveld, H.J., Uchida, T., 2006. Subsurface stormflow. Encycl. Hydrol. Sci. https://doi.org/10.1002/0470848944.hsa119.
Welch, S.A., Ullman, W.J., 1996. Feldspar dissolution in acidic and organic solutions: compositional and PH dependence of dissolution rate. Geochim. Cosmochim. Acta 60 (16), 2939–2948. https://doi.org/10.1016/0016-7037(96)00134-2.
Welsch, D.L., Kroll, C.N., McDonnell, J.J., Burns, D.A., 2001. Topographic controls on the chemistry of subsurface stormflow. Hydrol. Process. 15 (10), 1925–1938.
Western, A.W., Grayson, R.B., Blöschl, G., Willgoose, G.R., McMahon, T.A., 1999. Observed spatial organization of soil moisture and its relation to terrain indices. Water Resour. Res. 35 (3), 797–810. https://doi.org/10.1029/1998WR900065.
Whipkey, R.Z., 1965. Subsurface stormflow from forested slopes. Hydrol. Sci. J. 10 (2), 74–85.
White, A.F., Blum, A.E., 1995. Effects of climate on chemical weathering in watersheds. Geochim. Cosmochim. Acta 59 (9), 1729–1747. https://doi.org/10.1016/0016-7037(95)00078-E.
Willich, M., Buerkert, A., 2016. Leaching of carbon and nitrogen from a sandy soil substrate: a comparison between suction plates and ion exchange resins. J. Plant Nutr. Soil Sci. 179 (5), 609–614. https://doi.org/10.1002/jpln.201600036.
Xiao, D., Brantley, S.L., Li, L., 2021. Vertical connectivity regulates water transit time and chemical weathering at the Hillslope scale. Water Resour. Res. 57 (8). https://doi.org/10.1029/2020WR029207.
Zimmer, M.A., Bailey, S.W., McGuire, K.J., Bullen, T.D., 2013. Fine scale variations of surface water chemistry in an ephemeral to perennial drainage network. Hydrol. Process. 27 (24), 3438–3451. https://doi.org/10.1002/hyp.9449.